MINISTÉRIO DA CIÊNCIA E TECNOLOGIA
INSTITUTO NACIONAL DE PESQUISAS ESPACIAIS

INPE-14810-RPQ/261

BRAZILIAN DECIMETRIC ARRAY – BDA: THE FIRST LATIN AMERICAN DECIMETRIC INTERFEROMETER

H. S. Sawant[1], J. R. Cecatto[1], F. C. R. Fernandes[2], E. M. B. Alonso[1], M. C. Andrade[1], L. F. S. Cicconello[1], A. B. Cassiano[1], L. C. P. Moraes[1], F. R. H. Madsen[1], M. J. B. Silva[1], J. W. S. Vilas Boas[1], K. L. R. Souza[3], L. M. Costa[3], A. O. Souza3, R. R. Rosa[4], C. Faria[4,5], S. Stephany[4], J. D. S. Silva[4], L. B. T. Cividanes[6], C. A. I. Miranda[6], I. O. G. Vila[6], B. S. M. Correia[7], J. V. Vilas Boas[8], M. S. Ribeiro[8], N. Sato[8], L. C. L. Botti[9], C. M. Silva[10], J. H. Saito[11], C. E. Moron[11], N. D. Mascarenhas[11], I. C. Abrão[5], K. R. Subramanian[12], R. Ramesh[12], M. S. SundaraRajan[12], E. Ebenezer[12], G. Swarup[13], S. Ananthakrishan[13], M. R. Sankararaman[13], N. V. Nagarathnam[13], A. V. Sondur[14], D. E. Gary[15], W. J. Welch[16] and P. Janardhan [1,17]

1. *Astrophysics Division - DAS/INPE*
2. *Institute of Research and Development – IP&D /UNIVAP*
3. *BDA –Cachoeira Paulista / INPE*
4. *Laboratory of Applied Computer Sciences and Mathematics – LAC/INPE*
5. *Department of Computer Sciences, Univ. of Puc Minas – DC/PUCMinas*
6. *Division of Aerospace Electronics - DEA/INPE*
7. *Integration and Test Laboratory - LIT/INPE*
8. *Mechanical Designing Sector - SMD/INPE*
9. *Center of Radio Astronomy and Astrophysics, Univ. Mackenzie São Paulo – CRAAM/INPE*
10. *Neuron Electronics Pvt Ltd,. Brazil*
11. *Department of Engineering and Computer Sciences, Federal University of São Carlos. – DC/UFSCar*
12. *Inteltek Automation Pvt. Ltd. Pune – India*
13. *Indian Institute of Astrophysics, Bangalore – IIA, India*
14. *National Center of Radio Astronomy – NCRA/GMRT/TIFR, PUNE, India*
15. *New Jersey Institute of Technology – NJIT, U.S.A.*
16. *University of California, Berkeley – UCB, U.S.A.*
17. *Physical Research Laboratory, Ahmedabad – 380 009, India*

INPE
São José dos Campos
2007

MINISTÉRIO DA CIÊNCIA E TECNOLOGIA
INSTITUTO NACIONAL DE PESQUISAS ESPACIAIS – INPE

BRAZILIAN DECIMETRIC ARRAY – BDA: THE FIRST LATIN AMERICAN DECIMETRIC INTERFEROMETER

H. S. Sawant[1], J. R. Cecatto[1], F. C. R. Fernandes[2], E. M. B. Alonso[1], M. C. Andrade[1], L. F. S. Cicconello[1], A. B. Cassiano[1], L. C. P. Moraes[1], F. R. H. Madsen[1], M. J. B. Silva[1], J. W. S. Vilas Boas[1], K. L. R. Souza[3], L. M. Costa[3], A. O. Souza3, R. R. Rosa[4], C. Faria[4,5], S. Stephany[4], J. D. S. Silva[4], L. B. T. Cividanes[6], C. A. I. Miranda[6], I. O. G. Vila[6], B. S. M. Correia[7], J. V. Vilas Boas[8], M. S. Ribeiro[8], N. Sato[8], L. C. L. Botti[9], C. M. Silva[10], J. H. Saito[11], C. E. Moron[11], N. D. Mascarenhas[11], I. C. Abrão[5], K. R. Subramanian[12], R. Ramesh[12], M. S. SundaraRajan[12], E. Ebenezer[12], G. Swarup[13], S. Ananthakrishan[13], M. R. Sankararaman[13], N. V. Nagarathnam[13], A. V. Sondur[14], D. E. Gary[15], W. J. Welch[16] and P. Janardhan [1,17]

1. *Astrophysics Division - DAS/INPE*
2. *Institute of Research and Development – IP&D /UNIVAP*
3. *BDA –Cachoeira Paulista / INPE*
4. *Laboratory of Applied Computer Sciences and Mathematics – LAC/INPE*
5. *Department of Computer Sciences, Univ. of Puc Minas – DC/PUCMinas*
6. *Division of Aerospace Electronics - DEA/INPE*
7. *Integration and Test Laboratory - LIT/INPE*
8. *Mechanical Designing Sector - SMD/INPE*
9. *Center of Radio Astronomy and Astrophysics, Univ. Mackenzie São Paulo – CRAAM/INPE*
10. *Neuron Electronics Pvt Ltd,. Brazil*
11. *Department of Engineering and Computer Sciences, Federal University of São Carlos. – DC/UFSCar*
12. *Inteltek Automation Pvt. Ltd. Pune – India*
13. *Indian Institute of Astrophysics, Bangalore – IIA, India*
14. *National Center of Radio Astronomy – NCRA/GMRT/TIFR, PUNE, India*
15. *New Jersey Institute of Technology – NJIT, U.S.A.*
16. *University of California, Berkeley – UCB, U.S.A.*
17. *Physical Research Laboratory, Ahmedabad – 380 009, India*

INPE
São José dos Campos
2007

ACKNOWLEDGEMENTS

The hard task of successfully completing the development of the first phase of the BDA has been completed due to the dedication and hard work put in by the entire BDA team along with collaborators from national and international institutes. The enormous efforts made over the last four years has led to the development of the first Latin American Decimetric Interferometer for both solar and non solar observations. One dimensional solar map at 1.6 GHz have been successfully made.

The BDA team members would like to acknowledge here and extend their sincere thanks to all those who helped us in realizing this difficult task of development of the first Brazilian Decimetric Interferometer. The BDA is now a reality and we would like to extend our sincere thanks particularly to:

Dr. José Fernando Perez – Scientific Director, **Dr. Francisco Antonio Bezerra Coutinho** – Scientific Adviser , Mrs. **Virgínia G. C. Betim** – Scientific secretary , **Sr. Joaquim José de Camargo Engler** – Administrative Director of **FAPESP**. ***So also to referee's of the BDA project and all other authorities of FAPESP.***

Dr. Gilberto Câmara – Director of INPE, **Dr. João Braga** – Scientific Director of INPE, **Dr. Antônio L. Padilha,** Coordinator of Space and Atmospheric Sciences of INPE, **Dr. José Willians dos S. Vilas Boas,** Head of the Astrophysics Dept. and members of the Astrophysics Council and particularly to **Dr. J. H. A. Sobral**, ex-coordinator of the CEA-INPE and founder member of the BDA project.

Dr. R. Nityanand Director of National Centre of Radio Astronomy - Tata Institute of Fundamental Research (NCRA-GMRT-TIFR, Pune, India).

Mr. A. V. Soundar – President and **Mr. Sunil Raibagi** – Executive Director of INTELTEK AUTOMATION Co. Ltd., India.

Dr. R. Cowsik / Prof. Hanumath Sastry – Director/Acting Director of Indian Institute of Astrophysics, India, for supporting the development of the digital backend of the BDA and offering a donation to BDA – INPE, costing of about U$ 50.000,00.

Team members of the Computer Sciences of PUC-MINAS.

Respected Mr. **José Rui Hummel Mendonça**, Mayor of Cachoeira Paulista City and Mrs. **Maria da Graça Theodoro Diogo**, President of Municipal Camera.

Various technicians and employees of **the INPE at Cachoeira Paulista** for developing infrastructure for installation of the BDA antennas. In particular **Mr. Aluisio A. Silva –** Administrative officer, **Mr. Pedro P. Mota** – Electrical Engineer, **Mr. Ismar C. Filho e Mr. Carlos A. B. Lopes** – for helping in Topographic Survey of the BDA site and installation of computer network, respectively. **Mr. Armando Camara Jr.** – Manager of CPTEC computer network, **Mr. L. Francisco C. Marin** – Administrative officer of CPTEC computer network and **Mr. Sergio S. Rodrigues** - CPTEC Technician. Finally **Mr. Claudio Bressan** – Head of the Space Center of the (INPE-CP) and **Mr. Rubens Rocha** and his team members for cleaning and maintaining the land of the BDA project and keeping it clean and green. Our beloved Secretary **Mrs. Elaine C. P. Souza** for valuable administrative support to the BDA project.

To all national and international collaborators for participating and supporting in the development of the BDA project.

ABSTRACT

A team of Brazilian scientists are co-coordinating efforts to develop the Brazilian Decimetric Array (BDA) which is a 38-element radio telescope employing modern radio interferometric techniques and working in the frequency range of 1.2-6.0 GHz. The final baseline of the interferometer will be 2.27 km in the East-West and 1.17 km in the South directions, respectively. This instrument will obtain radio images from the sun with a spatial resolution ~ 4×6 arc seconds. A prototype of the BDA interferometer (PBDA), consisting of five antennas having base lines up to 220 meters in the East-West direction, operating from 1.2 – 1.7 GHz has been successfully put into operation for solar and non-solar observations at Cachoeira Paulista - CP – INPE (Latitude 45° 00' 20" West and Longitude 22° 41' 19" South) in the months of November – December 2004. The 6th antenna is currently being installed. Both, hardware and software were successfully tested for almost one year using observations of strong southern declination radio sources like Cygnus-A and the Crab Nebula. One dimensional brightness temperature maps of the sun at 1.6 GHz have also been obtained. In this report we give details of the procedures for amplitude and phase calibrations, estimated minimum flux detectable/beam, dependence of spatial resolutions on length of base lines, and a brief description of the hardware and its specifications. The estimated sensitivity of the PBDA consisting of 5 antennas of 4 m diameter each, is of about 3.5 Jy/beam for 1 minute of integration time for galactic and extragalactic observations at 1.4 GHz In case of the Sun, the estimated sensivities/beam for time resolution of 100 ms is around 880 SFU/beam (1 SFU = 10000 Jy). The BDA, when completed, will be open to the entire scientific community for use for both solar and non-solar observations and studies of space weather phenomena.

Table of Contents

LIST OF FIGURES

Pg.

LIST OF TABLES

Pág.

1 - INTRODUCTION

Scientists and engineers of INPE's Interplanetary Physics Group have, in the past, developed radio telescopes of international standards using available Brazilian technology. These telescopes are the Millimeter spectroscopes known as the Variable Frequency Millimeter Wave Radiometer, in operation since 1988 (Sawant et al., 1992a; Sawant et al., 1994; Cecatto, 1996), and the Digital Decimetric Brazilian Solar Spectroscope with a 9-meter polar mount antenna, in regular operation since 1990, at the INPE campus, The Brazilian Solar Spectroscope – BSS (Sawant et al., 1990; Sawant et al., 1991; Fernandes, 1992; Sawant et al., 1992b; Sawant et al., 1993; Sawant et al., 1996; Fernandes, 1997; Sawant et al., 2000a; Sawant et al., 2001; Fernandes et al., 2000a). The group has also initiated a Space Weather Prediction program using spectral tomography techniques in 1997 (Saito et al., 1996; Rosa et al., 1997; Rosa et al., 2000a, 2000b). Realizing the importance of imaging spectroscopy to solar terrestrial relationships and forecasting of space weather to the Brazilian space science program, a team of scientists/engineers initiated the design and planning of the Brazilian Decimetric Array project in 1996 (Sawant et al., 2000b, 2000c; Sawant et al., 2002; Sawant et al., 2003; Cecatto et al., 2004; Sawant et al., 2004; Faria et al., 2004; Sawant et al., 2007).

The Brazilian Decimetric Array (BDA), which is under development, will have high spatial and time resolutions of ~ 5 sec of arc (at 5.6 GHz) and 100 ms respectively. It is planned to employ modern technology at low cost to build the BDA. The BDA will have the capability of observing both solar and non-solar phenomena in the following protected radio bands *viz.* 1.2 - 1.7, 2.8 and 5.6 GHz. The sensitivity estimates show that the BDA will have an rms of 3 mJy at 21 cm for a system temperature of 50 K. The final version of the BDA will be an interferometric array consisting of 38 parabolic antennas of 4 meters diameter each with a compact "T" shaped array at the centre having 32 antennas. The array will be located at Cachoeira Paulista (45° 00' 20" West and 22° 41' 19" South).

The BDA will produce high spatial and time resolution images of radio sources with high dynamic range. The BDA will provide solar radio images to be used in a spectral tomography technique being developed for application to space weather forecasting. Using extensive Interplanetary scintillation (IPS) observations from the 4 station solar wind observatory at Toyokawa, Japan coupled with a tomographic mapping technique, some work has already been carried out in studying long lasting (> 24 hours) low density anomalies observed at 1 AU (Janardhan et al., 2005; Janardhan 2006). The analysis of such data will lead to a better understanding of the fundamental problems in solar physics and space weather. The BDA will also be very useful for galactic and extra-galactic investigations of the Southern hemisphere sky which is not accessible to VLA.

Here we describe in brief, the various phases of the development of the PBDA. Various aspects of the development of the prototype of the BDA consisting of a 5 element interferometer will be described along with details of electronic sub-systems such as front end, phase locked receivers, tracking system of alt–azimuth mounts of the 4 meter diameter paraboloid mesh type antennas, the digital correlator backend, the configuration of the PBDA antennas, amplitude and phase calibration, solar and non-solar observations and an example of one dimensional brightness distribution of the Sun on December 11th, 2004 at 1.6 GHz (Sawant et al., 2005) and its day-to-day variation at local noon (Ramesh et al., 2007).

1.1 - BDA Phases I and II.

The development of the prototype of the BDA project (Phase-I) began in December 2001 at the Brazilian National Space Research Institute campus at São José dos Campos, Brazil with base lines up to 32 meters. The main objective of the development of the prototype of the BDA (PBDA) project, consisting of a five element interferometer, was to develop the various

electrical, mechanical and electronic subsystems required and test them under operational conditions. The development of the PBDA would also help in optimizing and estimating the cost of various subsystems for mass production required for the subsequent stages. The PBDA was successfully completed in 2003 as shown in Figure 1.1. At the same time infrastructure like the required computing system and internet connectivity, civil, electrical engineering, protection against lightning and other facilities were developed in the site at Cachoeira Paulista. The 5 element PBDA interferometer was transferred to Cachoeira Paulista and set up with increased baselines of up to 220 meters in East-West direction as shown in Figure 1.2. Digital systems were interfaced in the month of December 2004 and solar and non-solar observations were carried out for about 45 hours during the period of November 22 – December 12, 2004. By 2009, we intend to add more 21 antennas (Phase-II) providing a maximum baseline of 256 m in East–West and 162 m in the South directions, respectively and constituting the "T" shape central portion of the array. In addition to this, topographic investigations were carried out over the whole area for setting up of the all 38 antennas of the final configuration of the BDA, distributed over distances of 2268-1170 m in East–West and South directions respectively. A number of private companies were involved in the development of the PBDA and efforts have been made to involve the same companies for further development of the BDA project and its annual maintenance. Regular operation and routine maintenance will be carried out by members and operators of the BDA team.

FIGURE 1.1 – Prototype of 5 element of BDA at INPE-**São** Jose dos Campos. The trailer is used as the control room.

FIGURE 1.2 – Prototype of 5 element of BDA at INPE-**Cachoeira Paulista** with increased base lines of up to 220 m in the East–West direction.

1.2 - Science with BDA

1.2.1 - Solar Physics

In the decimetric range two types of solar radio emissions are observed: i) a broadband emission due to gyrosynchrotron processes and ii) a group of narrow band fine structures due to various plasma mechanisms. Various fine structures lasting for couple of minutes are linked either with the pre-phase or impulsive phase of the solar flares. The first phase of the BDA (BDA-I) will provide positional information for long-lasting intense flares. This will enable decimetric activity to be associated with X-ray activity more accurately and hence will enable one to investigate, in a better way, the following problems: a) location of the acceleration region and process of particles acceleration (Sawant et al., 1990), b) chromospheric evaporation (Aschwanden et al., 1995), c) transport of energetic particles, and d) plasma emission mechanisms for various fine structures (Fernandes et al., 2000a, 2000b; Cecatto et al., 2003; Rosa et al., 1997, Rosa et al., 2002; Bastian et al., 1999; Ramaty e Mandzhavidze, 2000).

1.2.2 - Galactic and Extra-Galactic Studies

One can investigate the variability of Quasars and BL Lacertae objects as well as the classical Gigahertz Peaked-Spectrum (GPS) and Compact Steep-Spectrum (CSS) sources. With the high sensitivity and spatial resolution of the BDA one can study the morphology of extended radio sources like for example Centauris A and the Galactic Center. One can also study HI emission from extragalactic sources (ex. Galaxies with high star formation rate) as well as high velocity clouds in our galaxy. The BDA will be used to survey the radio sources in southern hemisphere and for continuum and line emission studies in the frequency range of (1 – 6) GHz. In our Galaxy giant molecular clouds are good sources to be investigated. The BDA will enable one to explore and study the dynamical properties of these clouds, particularly the dense component of the giant molecular clouds associated with extensive and compact HII regions.

The BDA will be adapted to investigate molecular lines of OH, as well as other molecular lines, in the our galaxy and also in the direction of comets and ultra-compacts HII regions.

Galactic foregrounds are a major issue in Cosmic Microwave Background (CMB) anisotropy and polarization studies and BDA observations can be used to delineate the foreground contaminants emission between 1.2 and 5.0 GHz. In particular, the Galactic emission in the frequency range between ~ 1 to 20 GHz is poorly known. We propose to coordinate joint and complementary observations using the GEM (Galactic Emission Mapping) telescope and BDA to investigate the diffuse Galactic emission and, specially, the so-called anomalous dust emission, in the frequency interval between 1 and 5 GHz.

2 - ELECTRONIC / ELECTRICAL / MECHANICAL SUB-SYSTEMS

2.1 - Front-end

Front-end consists of a dual polarized log-periodic feeder, a low noise amplifier (LNA) a high pass filter and a mesh type parabolic dish antenna of 4 meter diameter with an f/d ratio of 0.38.

2.2 - Low Noise Amplifires

The LNA operating in the frequency range of (1.2 – 1.7) GHz has been developed by using the Mini Circuits Lab chips T01217N having a noise figure ~1.5 dB a gain of ~25 db with a VSWR ~1.2 and with intermodulation of -30 dB. Each amplifier is put into thick metal boxes. The surface of the bottom plate of the metal box is used as heat sink. Two LNAs followed by high pass filters are connected to two ports of the log periodic antenna. Out puts of these filters are combined by combiner and sent to the receiver for down conversion. Two pin holes on the top plate allow for air circulation so as to avoid condensation caused by rapid fluctuations of the outside atmospheric temperature. Figure 2.1 shows the variation of gain and VSWR over the entire frequency range. The BDA site is in a valley thereby reducing RFI In addition to this a HP - 1000, high pass filter is connected after the amplifier and attenuates the signal below 1000 MHz, in particular, 900 MHz – the carrier frequency of mobile phones.

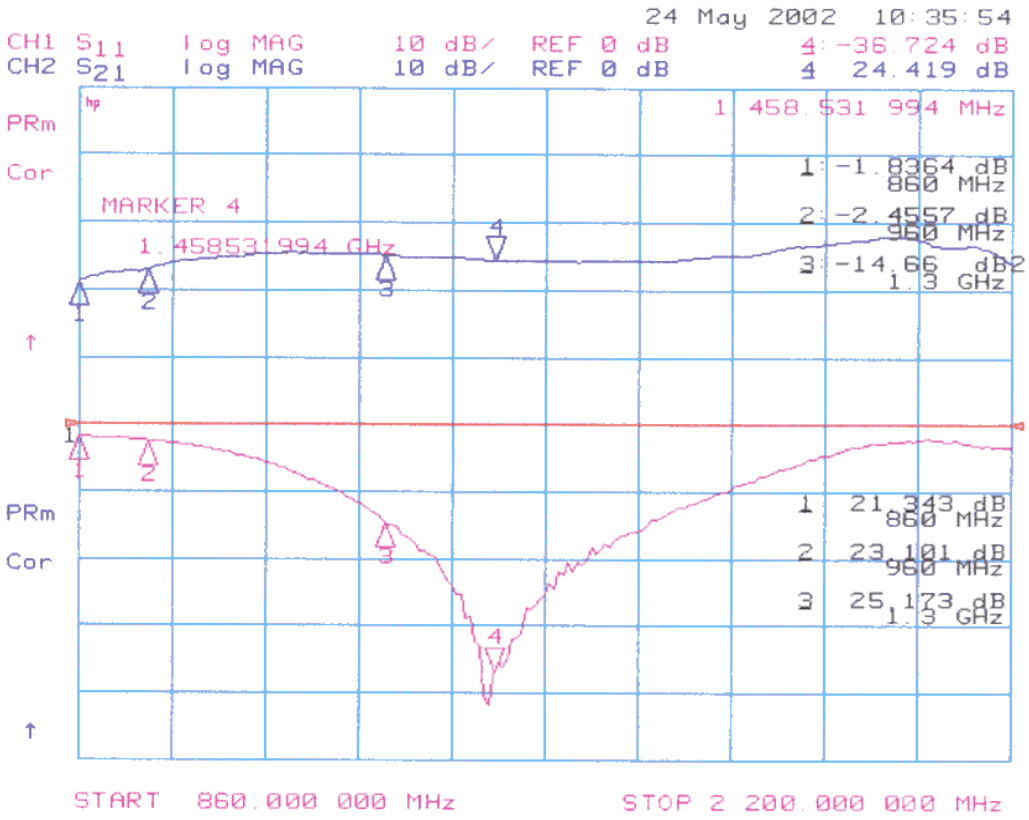

FIGURE 2.1 – Frequency vs. gain measurement (lower red curve) and VSWR (upper blue curve).

2.3 - Log-periodic dual polarized feeder (1.2 – 1.7) GHz

Crossed log-periodic dual polarized feeds have been developed at INPE for the 4 m mesh type parabolic dish, for prime focus mounting. The edge taper angle for the parabolic reflector having an f/d = 0.38 is given by

$$\varphi = 2 \times \arctan(1 \div (4 \times f / d)) \quad (2.1)$$

Electromagnetic waves are received by the antenna reflector surface and re-directed towards the focus. In the process, EM waves arriving at the focus undergo an amplitude variation (edge taper), depending on (the distance of the reflector from the focus). The primary beam response at the edge of the dish is added to the edge taper and is specified as the total taper loss. ρ , f and added edge taper loss, are related by the equation:

$$\rho = f \div \cos^2(\psi/2) \quad (2.2)$$

$$\text{edge taper} = \cos^2(\psi/2) \quad (2.3)$$

Using above equations one gets $\Psi = 66.7^{\circ}$ and 3.09 dB edge taper.

Radiation diagram for cosine squared type of the feeder optimum value of Ψ corresponds to 8 dB below the peak of the radiation diagram.

In view of reducing side lobes with illumination in H plane ~ 5 dB, with understanding that free space attenuation is ~3.1 dB. Designed log-periodic antenna is having directivity 7.3 dbi with following factor of antenna

Scaling factor $\tau = 0.90$

Relative space $\sigma = 0.06$

In order to operate in the desired frequency range, 8 elements are used in the feeder. In view of simplicity of production, the same diameter tubes are used for all elements. This affects the performance of the antenna very little. A Broad band balun is coupled to smallest element where antenna is illuminated. Other elements are adjusted so that phase difference between them is 180^0. These progressive phase inversions, direct the radiation pattern towards the smallest element. Eight dipoles consisting of two orthogonally separated elements are mounted in this manner with feeds as described above and shown in Figure 2.2. Five feeders, inserted in fibre glass radomes to prevent water from entering, were developed and tested at the focus of each antenna as shown in Figures 2.3 and 2.4.

2.4 - Measurement of radiation pattern

Measurements of radiation diagram were carried out in the Satellite Integration Laboratory of the INPE. The front-end was installed in a partially opened anechoic chamber so that it can receive the signals from a log - periodic antenna mounted on a 30 meter high tower, at the distance of 80 meter from anechoic chamber. This log periodic antenna was connected to a variable frequency transmitter. Tests were carried out at 1.2, 1.45 and 1.7 GHz. Figures 2.5 and 2.6 show the radiation patterns in the E and H planes for two polarizations. One can note that the attenuation in radiation diagrams for E and H planes are 15 dB and 5 dB as expected for $\Psi = 66{,}7^0$. In the operating frequency band (1.2 – 1.7) GHz, values of stationary waves for ports 1 and 2 are less than 1.8, and the gain is ~7.0 ± 0.8 dbi, with the cross talk being ~25 dB.

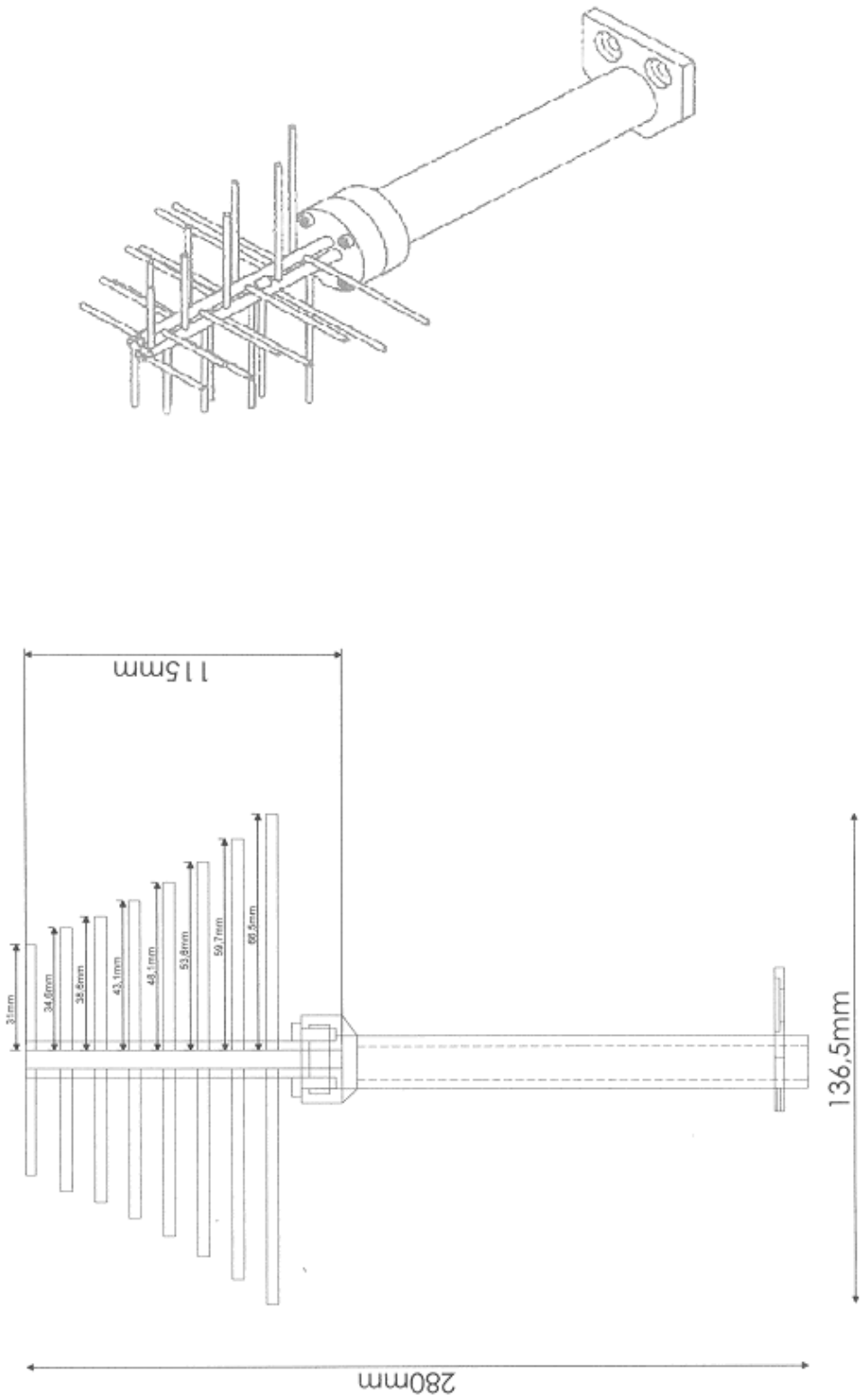

FIGURE 2.2 – Design of dual polarized crossed log-periodic antenna operating in the frequency range of 1.2 – 1.7 GHz.

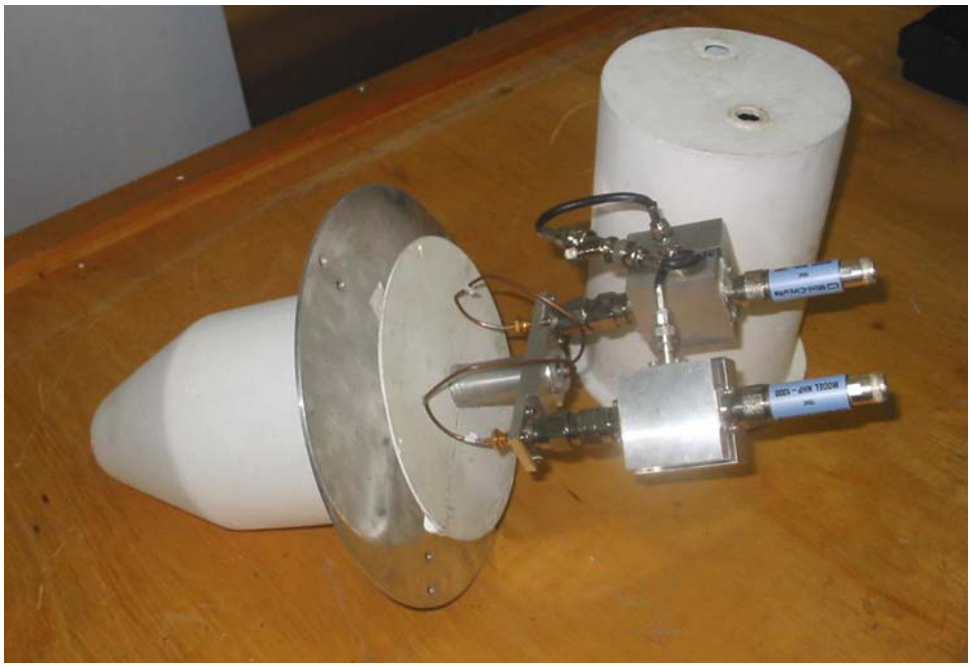

FIGURE 2.3 – The radome with the feeder inside. Ports 1and 2 of the feeder are connected to the LNA and high pass filter.

FIGURA 2.4 – Feeders with their respective radomes.

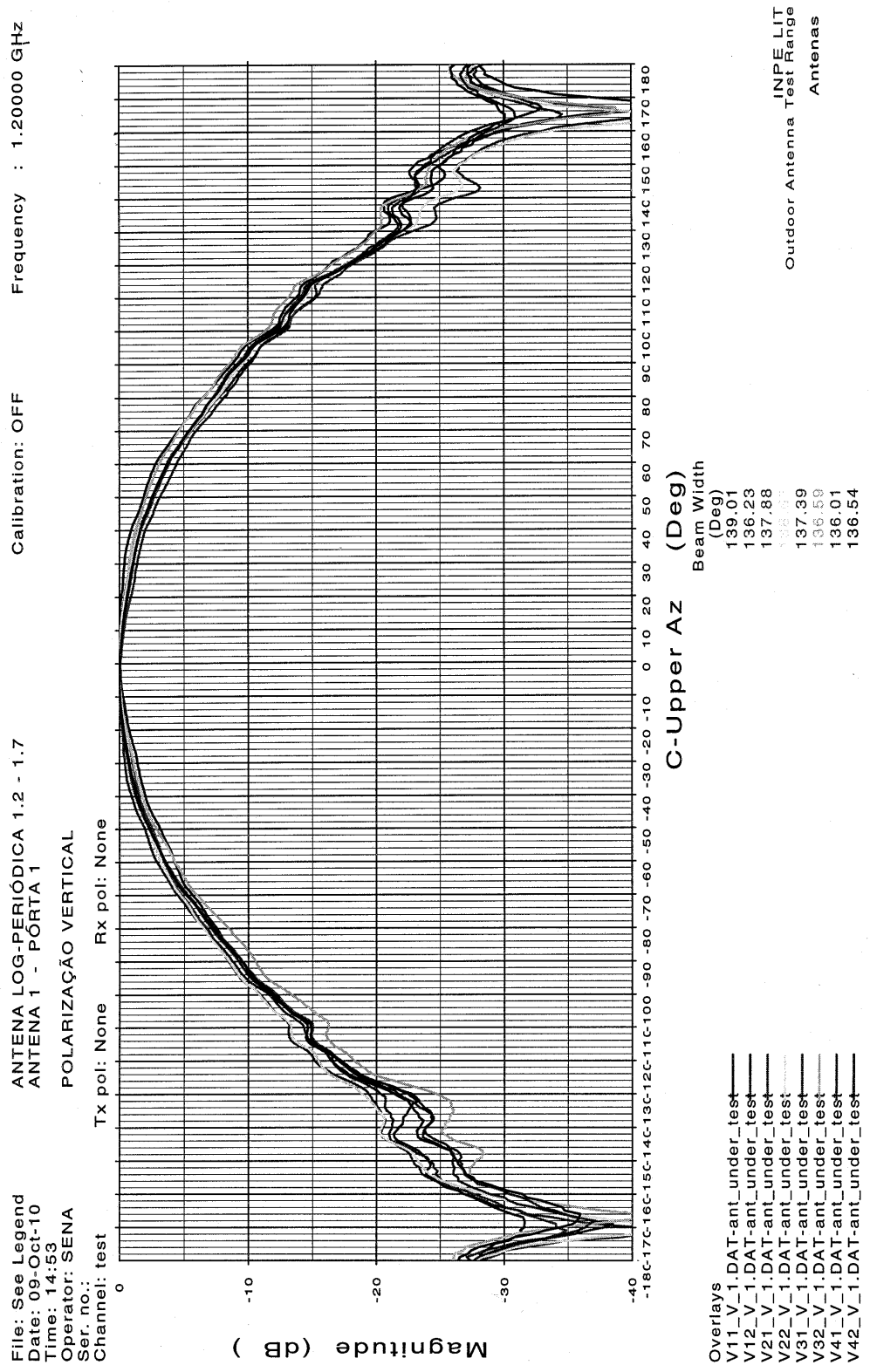

FIGURE 2.5 – Radiation diagram of the crossed polarized log-periodic feeder in the E planes for 4 antennas at 1.2 GHz.

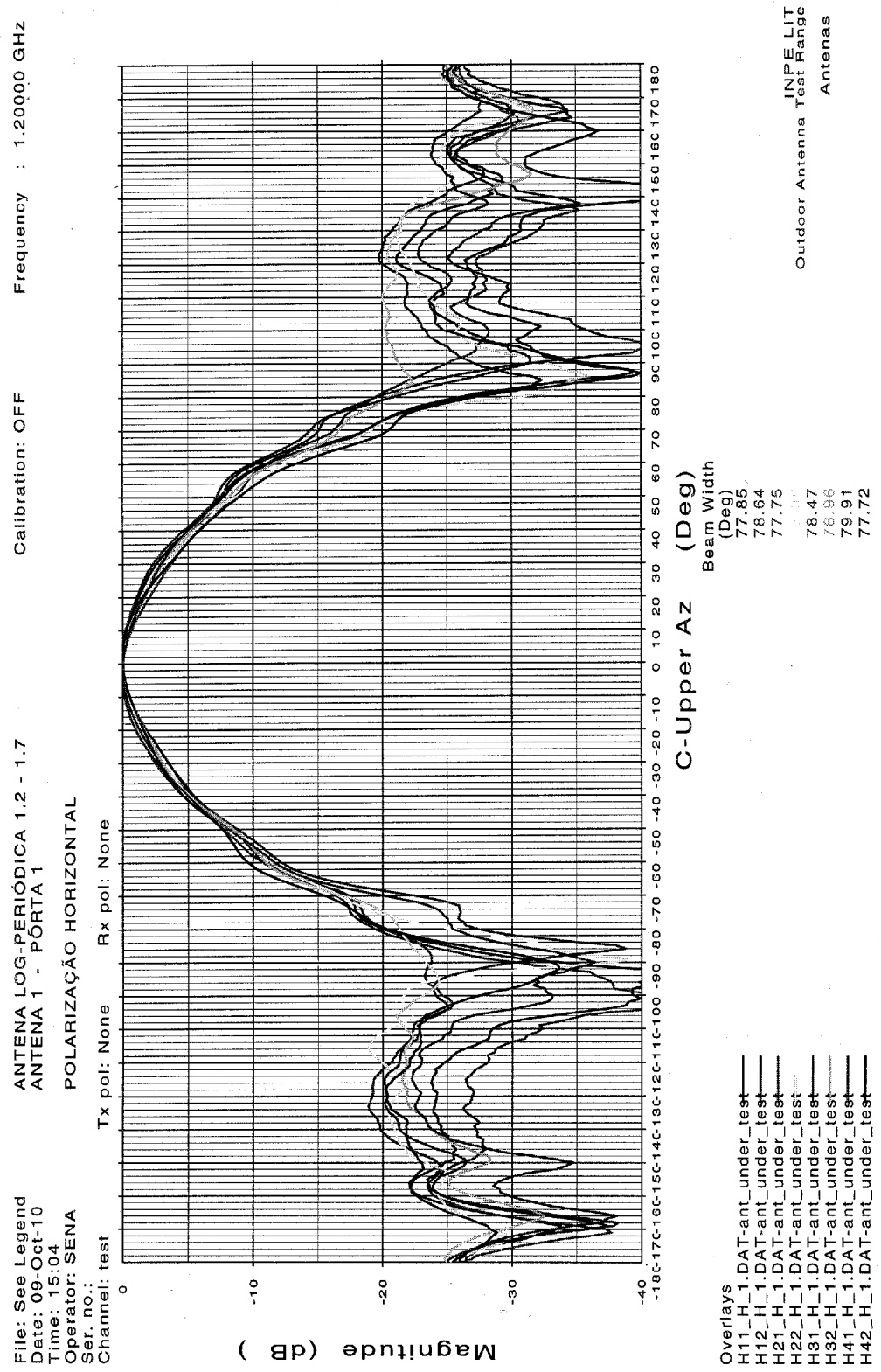

FIGURE 2.6 – Radiation diagram of the crossed polarized log-periodic feeder in the H planes for 4 antennas at 1.2 GHz.

3 - ALT–AZ MOUNT FOR 4 M DIAMETER PARABOLOIDAL ANTENNA

The antenna tracking system is the difficult and expensive part of the Brazilian Decimetric Array. The mechanical part of the alt–azimuth mount for the 4 meter paraboloidal mesh type antenna has been designed by Prof. Govind Swarup (1990, 1991) and is shown in Figure 3.1. AST–400 TECSAT 4 m diameter parabola is used and mounted on a mechanical tower with alt-azimuth mount designed by S&K Engineering Company (SKE) of Mumbai, India. The wind load factor, at various antenna positions, has also been taken into account during the design phase. All calculations have been provided by SKE for alt-azimuth/polar mounting. In addition to that, Prof. Swarup and SKE developed one antenna in India and it was tested by Brazilian and GMRT scientists, and given below are the technical specifications of the antenna. Characteristics of all subsystems were decided by taking into account wind pressure with different velocities and directions during antenna movements. It should also be noted that reduction of the self made noise of the electrical / electronic system was the major factors in deciding their specification.

3.1 - Technical specifications of alt-azimuth mount

1. Diameter of reflector — 4000 mm
2. Focal length — 1700 mm
3. f/d ratio — 0.38
4. h/d ratio — 0.147
5. Maximum wind speed — 120 km/hr
6. Operational wind speed — 60 km/hr
7. Reflector weights — 148 kg
8. Weight of supporting structure — 60 kg
9. Porosity of the dish — 0.33
10. Maximum pointing error — < 1 arc.min.
11. Limit switches — Non contacting type
12. Encoders — 12/ 16 bit
13. Steerability, speeds, motor capacity, gear ratio and torques, etc. (Table 3.1).

TABLE 3.1 - Stearability, speeds, motor capacity, gear ratio and torques.

Item	H.A.slew	H.A.Track	Declination	Azimuth	Elevation
Antenna speed	20^o/min	15^o/hr.	20^o/min	30^o/min	20^o/min
Design torque	300 kg m		200 kg m	200 kg m	200 kg m
Pinion ratio	10:1	10:1	10:1	10:1	10:1
Gear box ratio	100:1	100:1	100:1	100:1	100:1
Gear box output torque	36 kg m		24 kg m	24 kg m	24 kg m
Motor speed	60 RPM	0.7 RPM	60 RPM	60 RPM	90 RPM
Motor torque	45 kg.cm (630 oz in)		30 kg cm (420 oz in)	30 kg cm (420 oz in)	30 kg cm (420 oz in) -2 Nos.
Conter-weight	300 kg @ 1200 mm		150 kg @ 550 mm	Nill	70 kg-2 Nos.@ 850mm
Encoder	12 bit		12 bit	12 bit	12 bit
Limit. Switches	2 Nos.	2 Nos.	2 Nos.	2 Nos.	2 Nos.

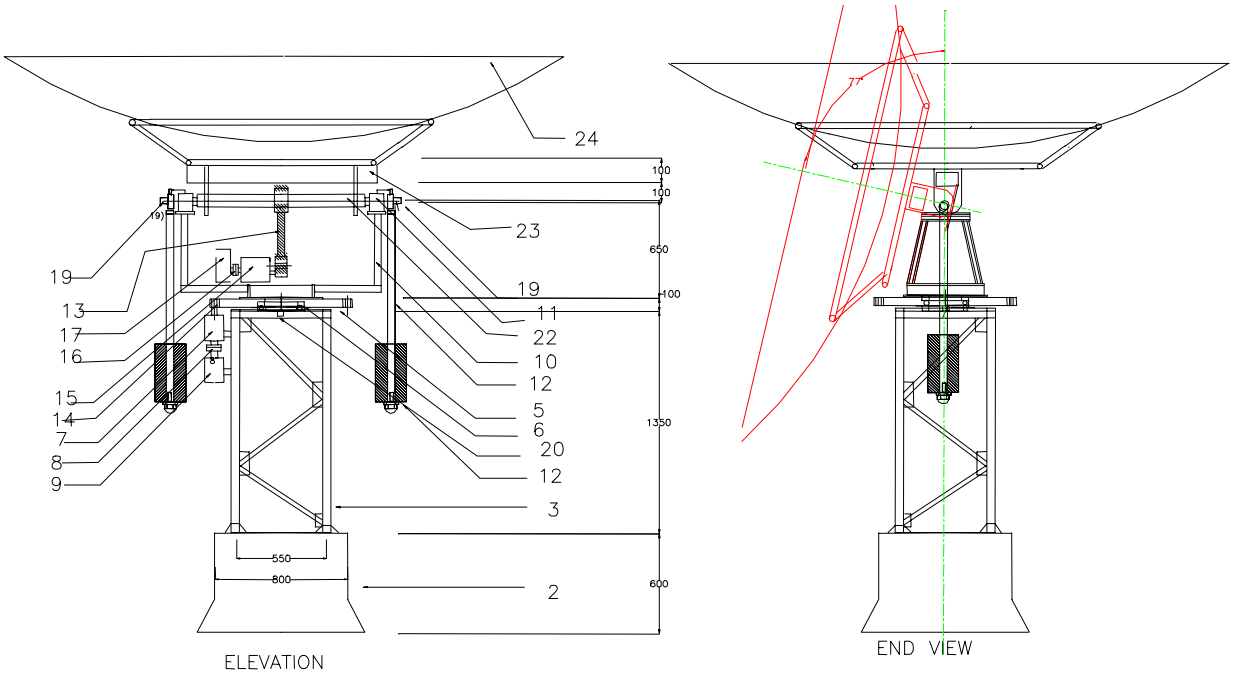

24	DISH	1	208Kg	024
23	BACK UP STRUCTURE	1	78.5Kg	023
22	EL.SHAFT	1	23.5Kg	022
21	AZ. ENCODER	1		021
20	EL. POTENSOMETER	1		020
19	EL. ENCODER	1		019
18	CWT. BLOCK	2	140.0kg	018
17	EL. MOTOR	1	4.0kg	017
16	EL.COUPLING	1	4.0kg	016
15	EL. GEAR BOX.	1	25.0kg	015
14	EL.PINNION	1	1.5kg	014
13	EL.BULL GEAR	1	60.0kg	013
12	CWT.ARM	2	22.0kg	012
11	EL.BEARING HOUSING&BEARING	2	40.0kg	011
10	YOKE	1	58.0kg	010
9	AZ. MOTOR	1	4.0kg	009
8	AZ. COUPLING	1	4.0kg	008
7	GEAR BOX	1	25.0kg	007
6	AZ.BEARING	1	11.5kg	006
5	AZ.BULL GEAR	1	100.0kg	005
4	BEARING BOTTOM PLATE	1	70.0kg	004
3	TOWER	1	100.0kg	003
2	FOUNDATION	1		002
1	ALT.AZ.MOUNT	1		001
SR.NO.	TITLE	QTY.	WT.	DRG.NO.

TITLE	ALT.AZ.MOUNT:-ASSEMBLY
DRG. NO.	SK/TIFR/INPE-001
DATE	8.11.1999
SR.NO	1/24

FIGURE 3.1 - Mechanical alt–azimuth mount and description of the various parts for the 4 / 5 meter diameter antenna.

3.2 - Specifications of motors

- AC brushless, synchronous motors having fast response to signals, less noisy.
- RPM between 0.6 and 600.
- Operating conditions - open field temperature 6^0 – 40^0 C, humidity between 60% and 100%, heavy showers with thunderstorms.
- Load on the motor is 3 Nm. Output and coupled reduction box with reduction ratio of 1/100, with out put of motor 300 N m.
- Capable of with standing torque of 600 Nm due to operational wind velocity ~ 60 km/h.

3.3 - Tracking system

Tracking system (Figure 3.2) has been designed by a private company known as Inteltek Automation Pvt. Ltd. – Pune jointly with engineers and scientists of GMRT – NCRA – TIFR – Pune – India.

Two servo motors are used to control each dish's tracking movements, to drive the azimuth and elevation axes. The designers of the positioning system on this project chose a Baldor NextMove-BX motion controller for the task, together with a combination of Baldor drives and brushless AC servo motors. Operating at just 0.6 RPM, the motors drive the loads through a combination of reduction and spur gearing to provide a positioning resolution of just 2.5 arc sec, at operating wind speeds of up to 60 km/hour.

The Next Move-BX motion controller is well suited to this task because of its combination of facilities, including dual axis capability, ruggedness for easy mounting underneath the antenna dish, and its built-in Mint motion language. Each of the 5 NextMove-BX units is linked to a host PC using a multi-drop RS-485 network. Running custom position control software, the PC transmits new position commands to the remote motion controllers at intervals of typically 60 seconds. The motion controllers' Mint application programs then autonomously provides interpolated movement commands to drive the azimuth and elevation servo motors, which ultimately move the axes at around one thousandth of a revolution per minute following gear reduction ratios of 800:1.

The first prototype alt-azimuth mount dish for this project was developed and tested in the month of May - June 2001 at NCRA- TIFR - Pune in India., with technical help provided by experts from the NCRA, who have extensive experience in this field. The measured accuracy of the positioning and tracking was less than 3 minutes of arc. While developing the prototype of five element interferometer, in Brazil, the type of gear and the gear ratios have been increased so as to further reduce the backlash. These modifications in the mechanical system have improved the pointing and tracking accuracy even for first phase of the BDA. In addition to that error correction measures will be incorporated in the system, which it is hoped, will further improve the accuracy, for the next phases of deployment.

Software consists of following main features for 5 antennas: man machine interface, networking (RS – 485), motion control software, auto mode, edit mode, diagnostic mode, manual mode, alarms, common control and remote control. This is based on MCS – 48 for controlling movements of the both axis following the commands of NEXT Move. Same time it will respond the command received from control tower by RS – 485 communication system.

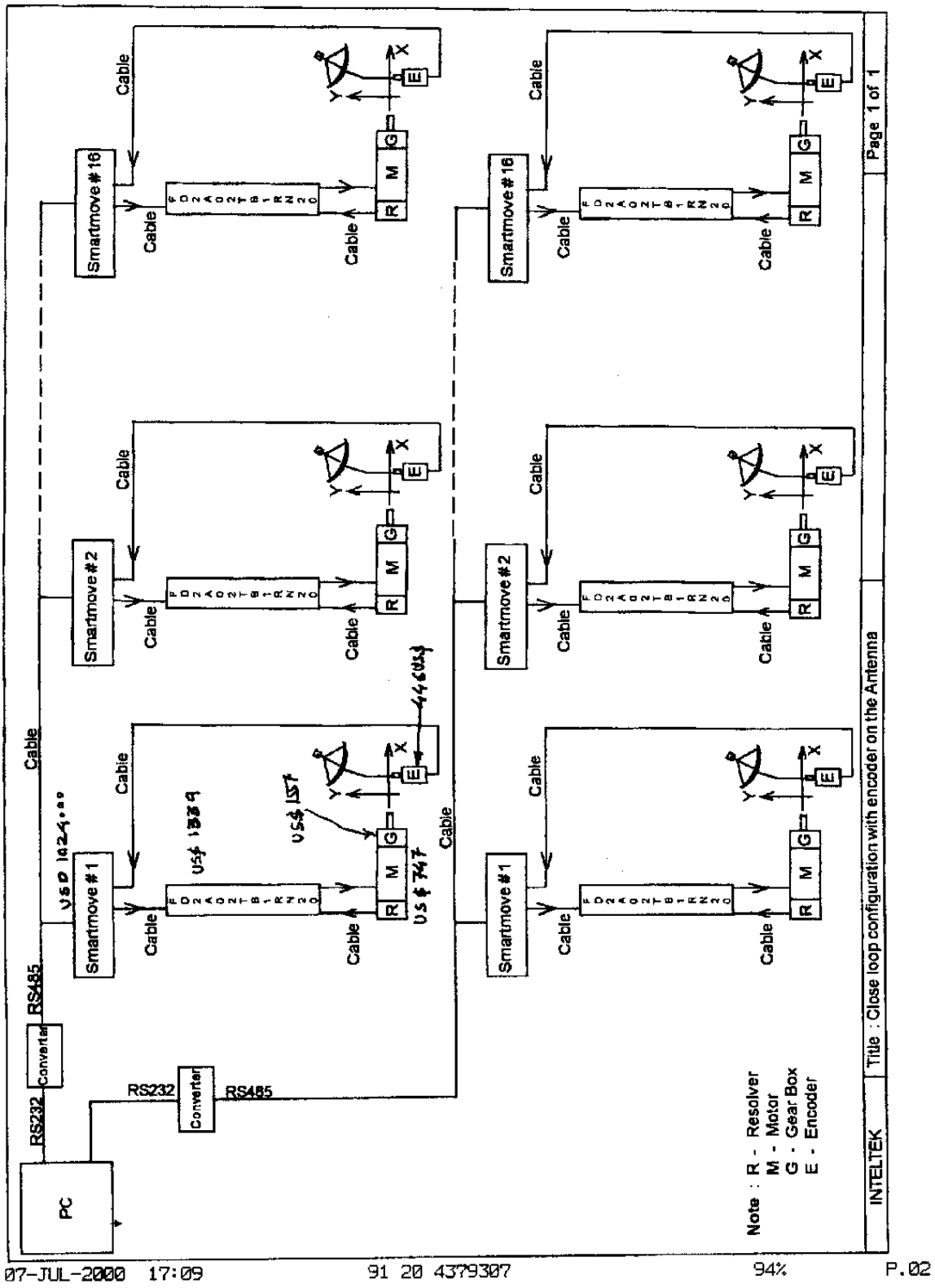

FIGURE 3.2 - Schematic of the electronic antenna tracking control system.

4 - RECEIVER

The PBDA has been set up in the city of Cachoeira Paulista and consists of five 4m alt–azimuth mounted parabolic antennas. Each antenna has its own amplifier directly connected to a feeder followed by HP - 1000 filter at the prime focus of the antenna. Observations can be carried out in the frequency range of 1.2 – 1.7 GHz. The out put of the LNA after the filter is sent to the receiver kept in the upper part of the supporting tower of the antenna. Here, after down conversion input frequency is converted to 70 MHz. This 70 MHz IF is sent to the control room located at a distance of ~125 m by shilded coaxial cable.In the control room 70 MHz is down converted to (0 - 2.5) MHz base band. This output is used to generate sine and cosine quadrature outputs.

Local oscillators at frequencies of 2050 – 2500 MHz, 906.5 MHz and 70 MHz, for triple down conversions of the input frequency are sychronised in phase and are generated at each of the antennas from a standard Rubidium clock of 10 MHz. A common 10 MHz, LO refrence signal is sent to all antennas. A dual-band based synthesiser unit at the antenna base, generates LO1 (2050 – 2500 MHz), LO2 (906.5 MHz) and in the control room LO3 (72.5 MHz). After the first down conversion, the signal is passed through a commercial band pass filter (BPF) (center frequency = 836.5MHz and usable bandwidth of 25 MHz) after which LO2 down converts the signal to the 70 MHz band. Finally, after passing through a BPF (center frequency = 70 MHz, 3dB BW = 5.35 MHz, 40 dB BW = 9.35 MHz) the LO3 downconverts the signal to the 2.5 MHz band.

The sysnthesiser chips have RF (RF1 or RF2) and IF sections. The quoted rms integrated phase noise error (100 Hz to 100 kHz) for each section, are i) RF1 and RF2 sections: 1.2/1.0 deg, and ii) IF section: 0.4 deg, respectively. These are indicative figures and are not actual temperature stability. The phase noise in RF bands at 1 MHz offset, is -130 dBc/Hz and – 131 dBc/Hz, respectively. In the IF band it is – 104 dBc/Hz at 100 kHz offset. The chip is capable of operation between -40^0 C and $+85^0$ C.

For convenience the receiver is divided into 4 blocks. Figure 4.1 shows the function and location of each block where as Figure 4.2 shows details of the each block, with input output frequency and their gains and other parameters, such as loss in the cables while sending and receiving signals. In these figures, apart from indicating functions of the various blocks the gain of the amplfiers, the frequency conversions, the characteristics of filters etc. are also mentioned. Also, the locations of each block are indicated.

Figures 4.3 and 4.4 show, respectively, the location of the receivers parts kept in the tower of the antenna and in the container – control room. Table 4.1 indicates the main components of PBDA receiver and their functions. Frequencies and required power levels for down convesions are shown in Table 4.2.

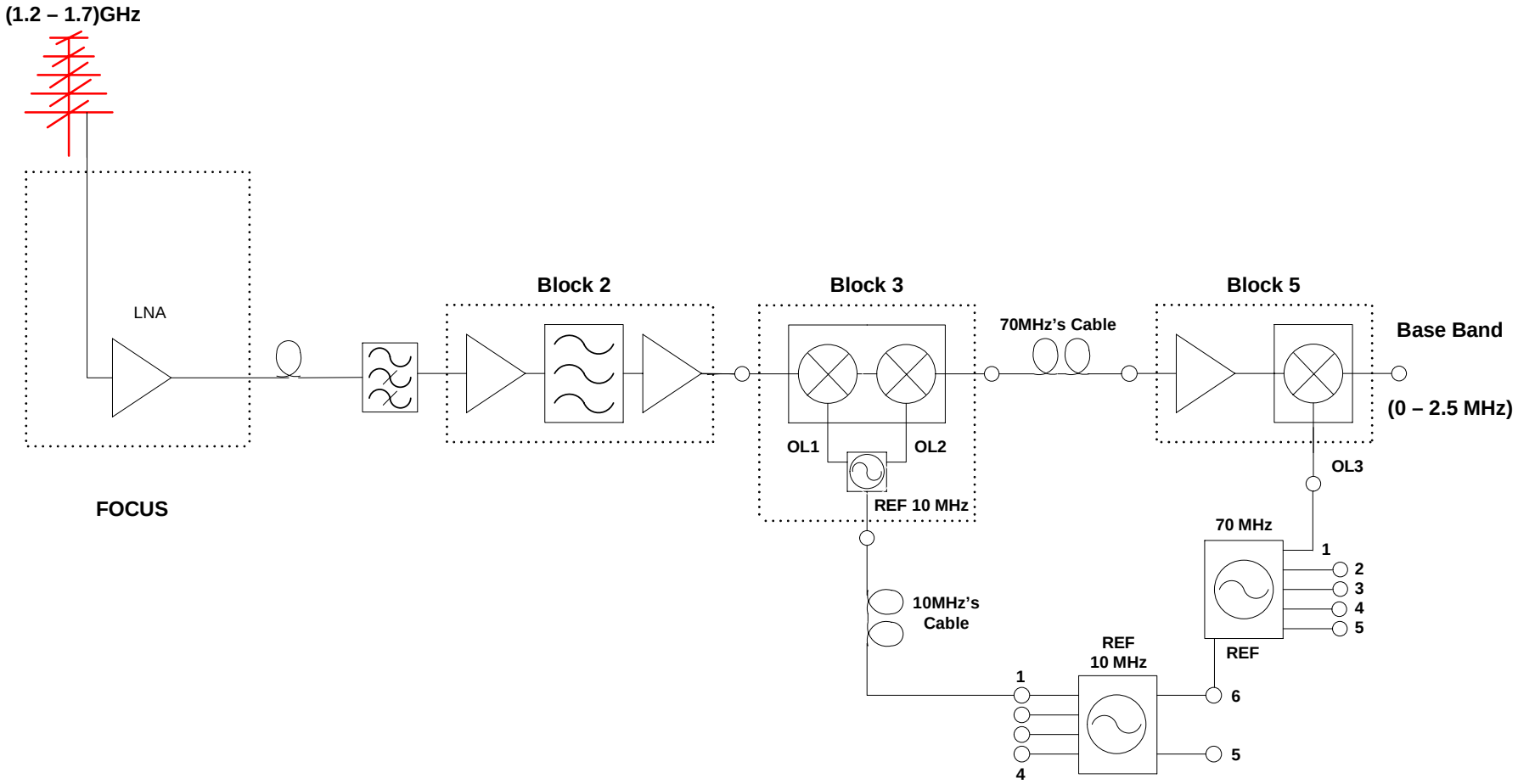

FIGURE 4.1 – Block diagram of the PLO type receiver operating in the frequency range 1 - 6 GHz, including the signal distribution of LO to the 38 antennas.

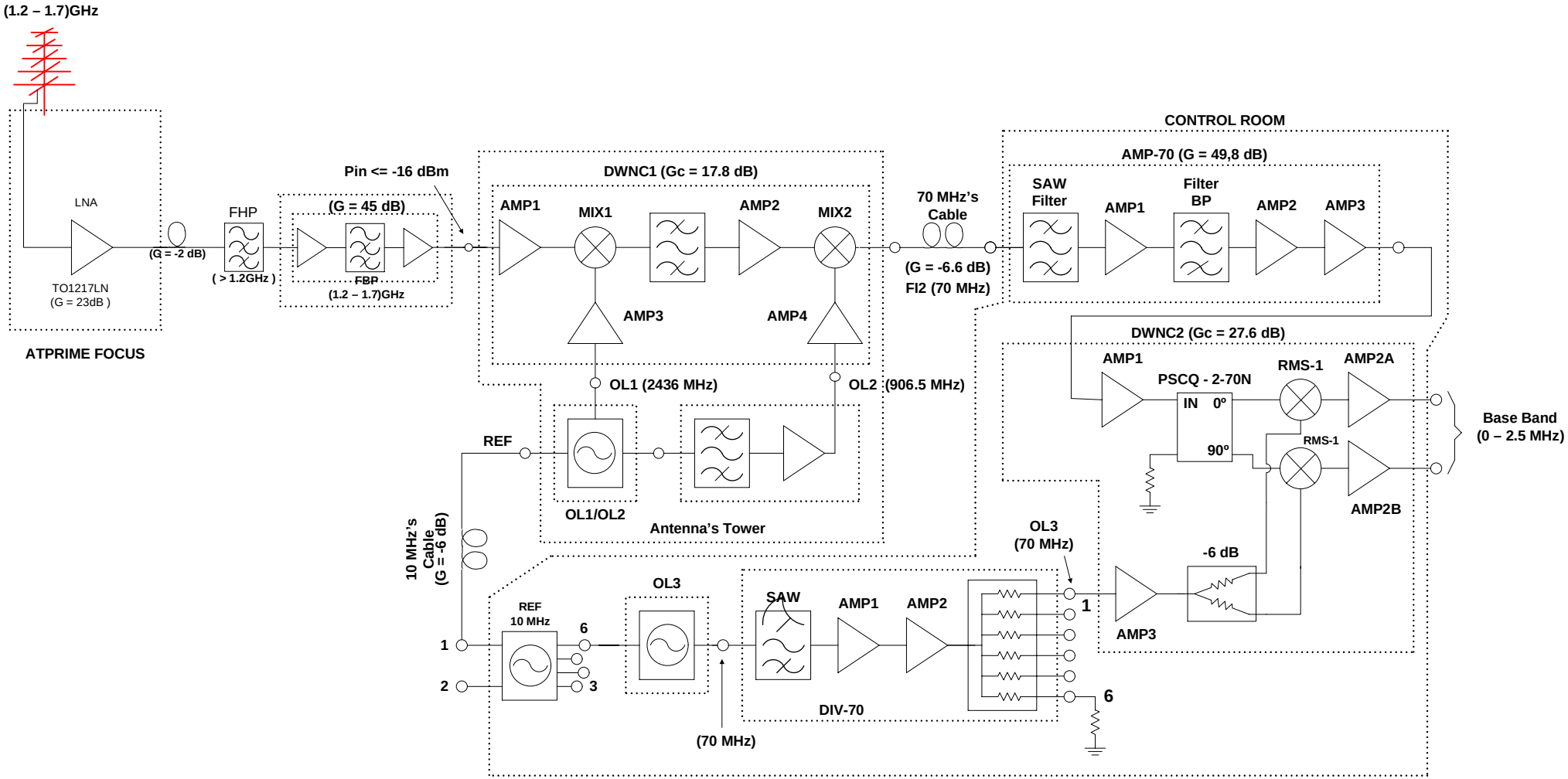

FIGURE 4.2 – Details of the figure 4.1.

FIGURE 4.3 – Photo of the receiver part in the tower of the antenna. The input frequency is 1.6 GHz and the output frequency is 70 MHz.

FIGURE 4.4 – Photo of the 5 receivers in the control room. The input frequency is 70 MHz and the output frequency is 2.5 MHz.

TABLE 4.1 – Main receiver components indicated in the block diagram.

Shortform	Function	Location	Function
LNA	Low Noise Amplifier	Prime focus of the antenna	Noise Figure 1.5 dB amplifier with gain ~25 dB (1.2 – 1.7) GHz
DWNC1	DoWN Converter #1	Base of the antenna	Double down conversion to IF of (70 ± 2.5) MHz
AMP-70	Amplifier at 70 MHz	Container	Amplifier IF
DWNC2	DoWN Converter #2	Container	Down conversion of 70 MHz to (0 - 2,5 MHz) base band
OL1/OL2	Local Oscillator #1/ Local Oscillator #2	Base of the antenna	Generate signals of L01 and LO2 for double down conversion
OL3	Local Oscillator #3	Container	Generate signal of LO3
AMP-906	Amplifier at 906,5 MHz	Base of the antenna	Amplifier of LO1 and LO2 signals
DIVP-70	Power Divider at 70 MHz	Container	Amplifier of 70 MHz IF and 5 way divider
REF 10 MHz	REFerence of 10 MHz	Container	Rubidium clock at 10 MHz signal sent to the frequency synthesizer to generate LO1, LO2 and LO3

TABLE 4.2 – Frequencies and required power levels for the down conversions.

Signal	Component	Frequency MHz	Power in dBm
LO1	DWNC1	2436.0	-5.8
LO2	DWNC1	906.5	-10.5
LO3	DWNC2	70.0	0 *
REF 10 MHz	LO1/LO2, LO3	10.0	ASD

Initial testing of 2 elements of the BDA interferometer were done, in additive and multiplicative mode by observing the Sun, at 1.5 GHz, with a baseline of 24 m using an analogue multiplier. Fringes with expected separation ~1.91 minutes in time were obtained for the first time on 8th Feb. 2003. The efficiency of the analogue correlator obtained was 66% as expected.

4.1 - Electronic system for programming frequency synthesizer up to distances of 400 m

A communication system between control PC and frequency synthesizer and vice-versa up to distances of 400 meter by using three MAX 3491 chips connected by cable (generally used for internet connections) was developed as shown in Figure 4.5. From parallel port of the control PC, command signals are sent to the frequency synthesizer to generate the desired frequency. A similar system is connected to the parallel port of the frequency synthesizer. Two-way communication is establish between them, as shown in Figure 4.6

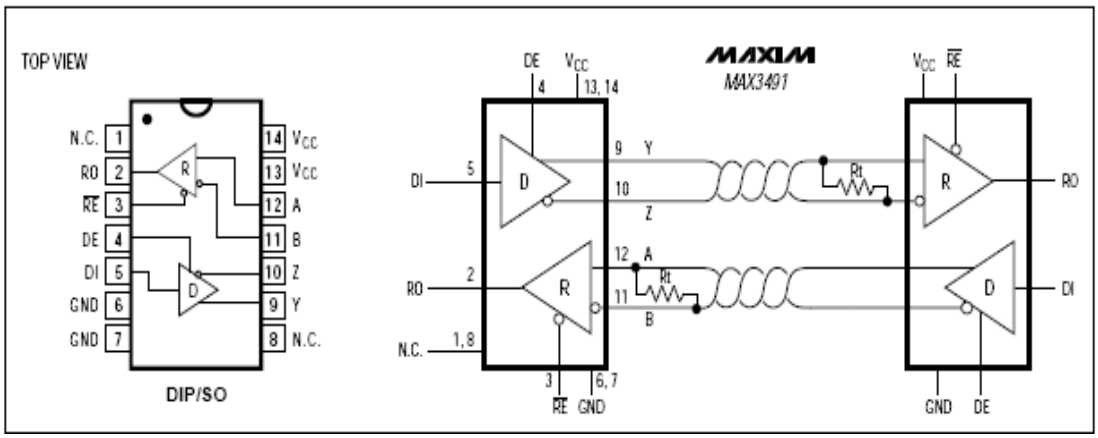

FIGURE 4.5 – Configuration of chip MAX3491 communicating with frequency synthesizer.

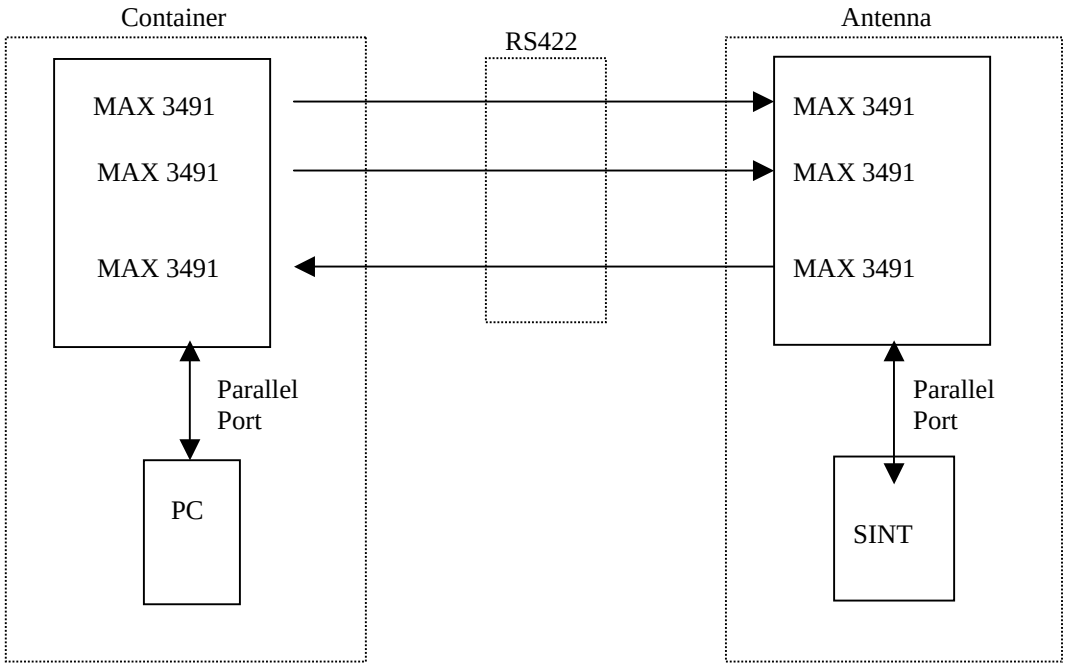

FIGURE 4.6 – System for remotely controlling frequency synthesizer.

4.2 - Estimated sensitivity of PBDA, in units of flux density

According to Walker [1989], the sensitivity of an array of N identical antennas is,

$$\Delta I = \frac{2k\,T\,\eta_b}{\eta\,A\sqrt{N_b \tau \Delta \nu}} \qquad (4.1)$$

where k is the Boltzmann constant, T_{sys} is the system temperature, η_b is a factor corresponding to loss in various stages of the antenna/receiver system, η is the aperture efficiency, A is the

physical area of each antenna, $N_b = N_a \times (N_a\text{-}1)/2$ [where N_a and N_b are the number of antennas and baselines, respectively], τ - integration time, $\Delta\nu$ - final I.F. bandwidth.

$$\text{With } T = (T_a^{\,2} + T_a\, T_{sys} + \tfrac{1}{2}\, T_{sys}^{\,2})^{1/2} \qquad (4.2)$$

where T_a is the antenna temperature due to source contribution, T_{sys} is a sum of several noise contributions which are microwave and galactic backgrounds emission, T_{back}, atmospheric emission, T_{sky}, ground radiation scattering into the feed, T_{spill}, loss in the feed, T_{loss}, injected calibration signal emission, T_{cal}, and receiver noise temperature including the contributions from the second and following stages, T_{rec} (T_{LNA} + temperature of secondary stages). We know that $NF_{LNA} \approx 1.5$ ($T_{LNA} \sim 150$ K) and $G_{LNA} = 23$ db. Assuming upper limits for $T_{back} \approx 25$ K, $T_{sky} \approx 25$ K (Kraus, 1986, p. 7-1, assuming 50% aperture efficiency), and other contributions are negligible we obtain

$$T_{sys} = T_{rec} + 50 \text{ K, with } T_{rec} = T_{LNA} + 1/G_{LNA}\, T_{RF} \qquad (4.3)$$

Where, T_{RF} encloses temperature contributions from all receiver electronics other than LNA.

Since LNA has a high gain (23 dB) we can assume $T_{rec} \approx T_{LNA} = 150$ K. Hence, $T_{sys} = 150 + 50 \approx 200$ K.

If we are observing a weak extra-galactic source then, $T_{sys} >> T_a$, $T \sim T_{sys}/\sqrt{2}$, and we obtain:

$$\Delta I = 2k\, T_{sys}\, \eta_b / (\eta\, A \sqrt{2 N_b \tau \Delta\nu}) \qquad (4.4)$$

An example that can be taken is Cygnus-A whose flux density at 1.6 GHz is approximately 1400 Jy which means a $T_a \approx 3.5$ K.

In this case, assuming natural weighting and using $k = 1.38 \times 10^{-23}$ J/K, $\eta_b \sim 2$, $\eta = 0.5$, $A = 12.6$ m^2, $N_b = 10$, $\Delta\nu = 2.5$ MHz., we obtain an upper limit of $\Delta I \approx 25$ Jy/beam, using 5 antennas with 1 second time integration. Now, in case we use 6 antennas the upper limit falls to $\Delta I \approx 20$ Jy/beam.

For a strong source, like the Sun, $T_{sys} << T_a$, then from (1) and (2) we get $T \sim T_a$

$$\Delta I = 2k\, T\, \eta_b / (\eta\, A \sqrt{N_b \tau \Delta\nu}) \qquad (4.5)$$

However, for PBDA 4 m dish we have a FWHM = 3.28°. In this case the Sun has a diameter of ~ 0.5 degree, which can be considered a point source. Therefore, we have $T_a = T_B \times \Omega_{Source}/\Omega_{Antenna} = 2.32 \times 10^{-2} \times T_B$. Taking $T_B = 63.8 \times 10^3$ K at 1.6 GHz (according Zirin et al, 1991), then $T_a \approx 1480$ K, and using expression (2) with $T_{sys} = 200$ K given above we obtain $T \sim 1580$ K.

Finally, for observations of the Sun at 1.6 GHz using 5 antennas with $\Delta\nu = 2.5$ MHz and 0.1 sec time integration as well as previously calculated parameters we estimate (1) an upper limit of $\Delta I \approx 880$ Jy/beam = 0.088 SFU/beam. A value of $\Delta I \approx 720$ Jy/beam = 0.072 SFU/beam is obtained in the case we use 6 antennas.

5 - DIGITAL SYSTEM

5.1 - Introduction

In its present form, the PBDA has 5 antennas arranged along the E-W direction and operates in the one-dimensional mode. Correlations are performed for all the antenna pairs and to get 22 real outputs (1 cosine and 1 sine output for each interferometer pair). Two of the above outputs correspond to total power measurement. As the information content of the celestial source is contained in the complex visibility observed with an interferometer, the above 20 outputs are arranged to form 10 complex visibilities, pertaining to the 10 different baselines in the array. The above visibilities are obtained using 1-bit, 2-level correlators (Weinreb, 1963) which can be assembled using simple digital logic and yields greater stability to the backend receiver than an analog correlator.

The following sequence of operations is performed in the backend receiver system of the BDA. The signal from the I.F. amplifiers in the last stage of the analog receiver system are first passed through a digitally controlled phase switching unit (PAS-1 of Mini-Circuits mc., USA) in the control building, i.e. Walsh switching (Beauchamp, 1975). Then they are quantized to two levels in a zero crossing detector. The basic element used here is a high speed comparator (AD 790). The output of the comparator is a 'TTL' signal corresponding to whether the input I.F. signal is above or below the 'ground' level. The quantized signal is then sampled in a D-type flip flop (74L574) at a rate of 5 MHz (Figure 5.1), the Nyquist rate corresponding to the final I.F. bandwidth (2.5 MHz) used in the BDA. An Ex-OR gate (74L586) is used to demodulate the sampled signal for Walsh switching. After the removal of phase inversion, the signal then flows through the delay lines constructed using a combination of shift registers (74L5 164) and multiplexers (74L5151). The necessary delay is implemented under the control of a computer instep of 0.2 μs up to a maximum value of 3 μs. This enables us to carry out observations of sources located even at large distance from the zenith by applying proper corrections for the geometrical delay suffered by the different antennas.

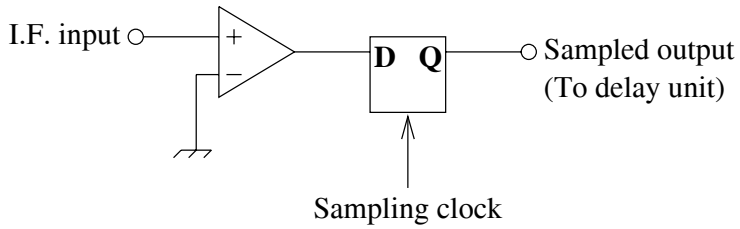

FIGURE 5.1 – Block diagram of 1-bit sampler.

The correlator system was built using the chips primarily designed for the Nobeyama radioheliograph, Japan (Nakajima et al., 1993) and the Gauribidanur radioheliogaph near Bangalore in India (Ramesh et al., 1998). These are custom built chips using CMOS gate array technology. The architecture of the chip is shown in the Figures 5.2 and 5.3. Each chip can accommodate 4 antennas. For example, if the signal from antennas 1, 2, 3 & 4 are fed at its input, then the output will be the correlation between the following antenna pair: 1 × 2, 1 × 3, 1 × 4, 2 × 3, 2 × 4 and 3 × 4. If C_1, S_1 and C_2, S_2 are the cosine and sine I.F. outputs of antennas 1 & 2, then each cosine and sine correlator will give output according to $C_1 \oplus C_2 + S_1 \oplus S_2$ and $C_1 \oplus S_2 - C_2 \oplus S_1$, respectively. At the end of every integration period (100 ms), the data from the different correlators will be written into a memory unit.

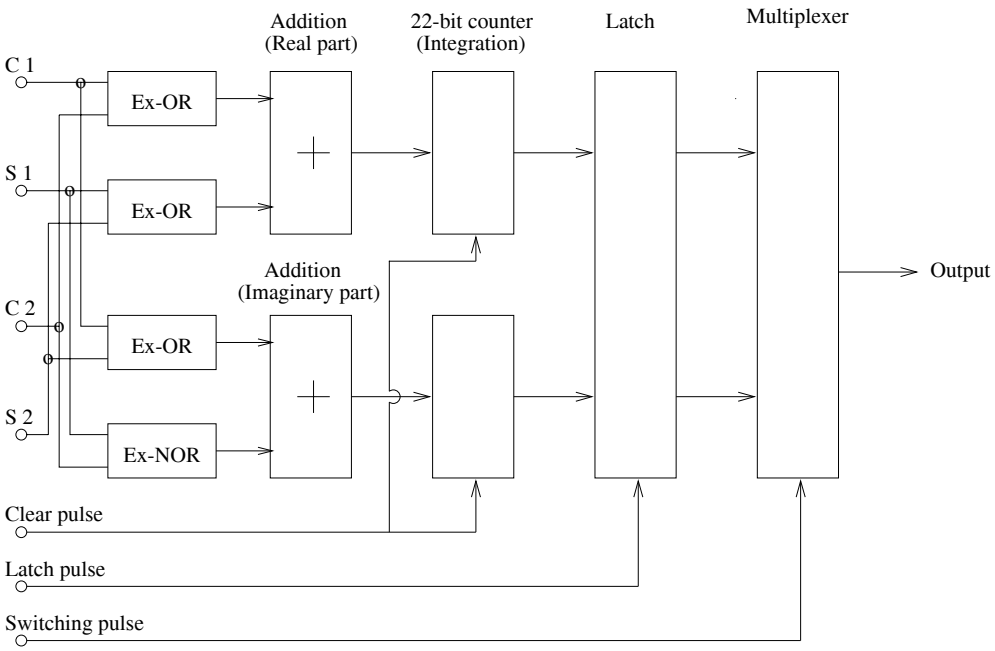

FIGURE 5.2 – An elementary circuit of the correlator chip.

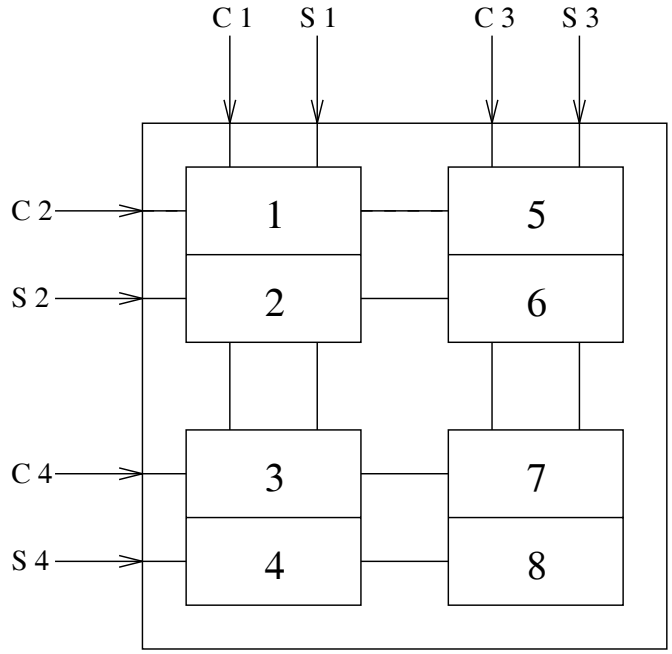

FIGURE 5.3 – Functional diagram of the correlator chip.

Note that there are two such units in the BDA correlator system. The process of reading correlated data and writing into the memory unit goes on till we reach 256 integration cycles. During this time, i.e. when data is written into one memory unit, the data that was written into

the other memory unit during the earlier 256 integration cycles will be read into a computer. At the end of 256 integration cycles, the role of the memory units get reversed (Ramesh, 1998).

5.2 - Total power measurement

The use of 1-bit correlator results in a loss of the amplitude information of the input signal. The latter are digitized as either +1 or 0 (in some cases +1 & -1) depending on whether it is above or below the threshold level of the comparator. So information on the absolute strength of the signal will be lost (like in correlator systems with an Automatic Gain Control loop), as only the sign of the input waveform is retained. The output of a one-bit correlator is proportional to the ratio between the power of the correlated and the sum of the correlated plus uncorrelated signals at its input, i.e. it measures the normalized correlation coefficient unlike an analog correlator where the output is proportional to the correlated signal from the source.

If T_s is the source brightness temperature and T_b is the sky background temperature in the direction of the source, then the measured correlation coefficient (ρ_m) is given by (Figure 5.4)

$$\rho_m \propto \frac{T_s}{T_s + T_b} \tag{5.1}$$

Hence in order to get the true correlation coefficient (αT_s), the total power received by the antenna (i.e. $T_s + T_b$) has to be measured separately and multiplied with the measured correlation coefficient in equation 5.1. The conventional techniques to measure the strength of the input signal require square-law detectors, A/D convectors, etc. Also, it will be difficult in synchronizing the data acquisition with the correlator system. One can configure the 1-bit correlator chip itself to measure the strength of the input signal and this way the set-up can be included as a part of the digital backend receiver as shown in Figure 5.5 (see UdayaShankar, 1986; Ramesh et al., 1998 for details on this topic). In addition to the loss in amplitude information, the sensitivity of a 1-bit correlator is only 64% compared to the analog case (Van Vleck and Middleton, 1966). But this loss of sensitivity is not severe in the case of solar observations since the received signal is usually strong. Figure 5.6 shows the total power from the Sun measured using the above setup.

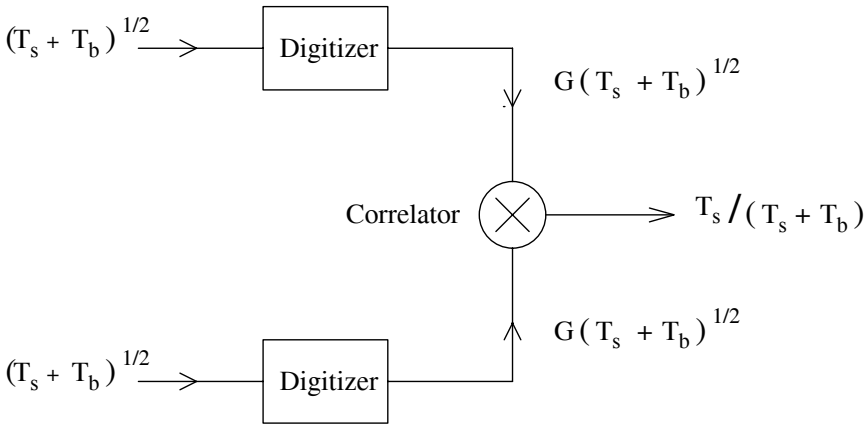

FIGURE 5.4 – Output of a one-bit correlator.

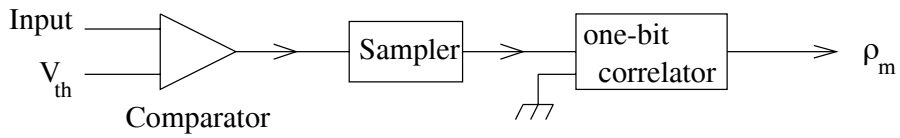

FIGURE 5.5 – Set-up to measure the total power using the PBDA one-bit correlator.

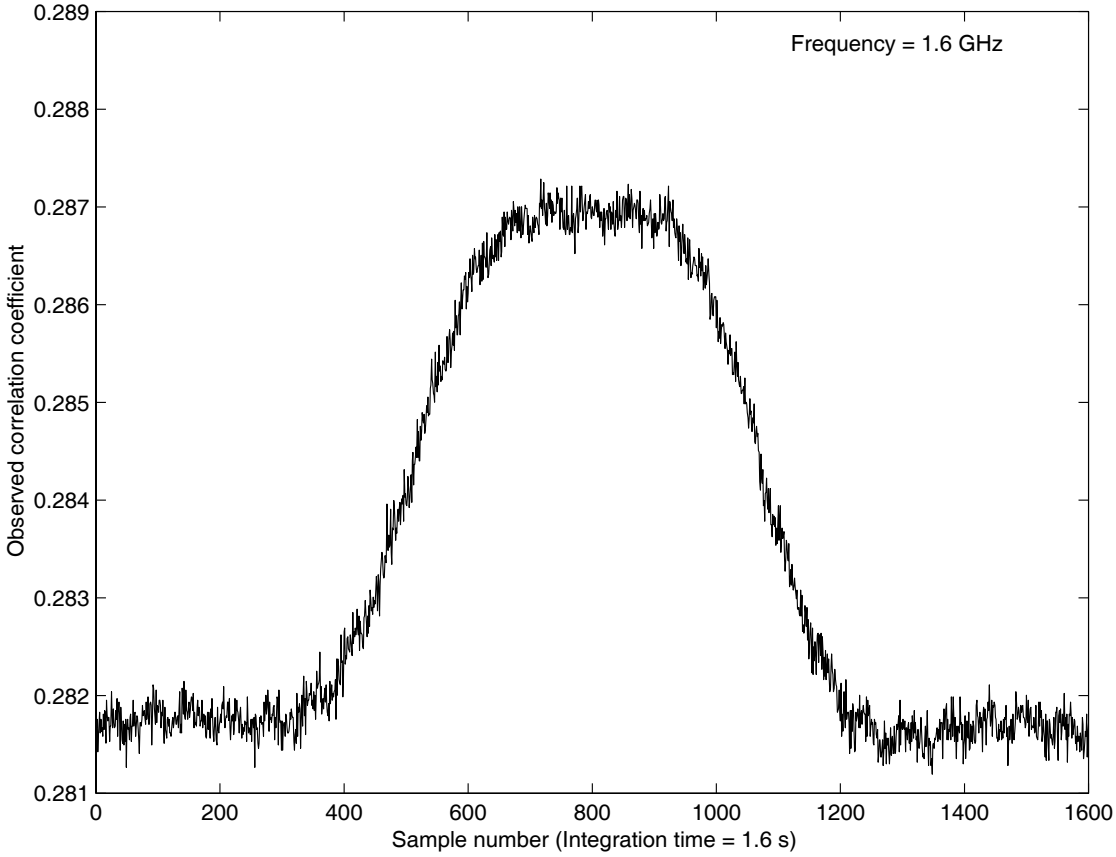

FIGURE 5.6 – Total power from the Sun measured with the PBDA antenna 1 on December 9, 2004.

5.3 - Walsh switching

The coaxial cables used for transmitting the I.F. signal from the antenna base to the control room are well shielded. Also, the cables in the analog receiver rack inside the building are separated. Proper care has also been taken while making the 'ground' of the power supply to the digital receiver unit. However, inspite of these precautions, there is always the possibility of a certain amount of crosstalk between the individual signal channels which could give rise to spurious correlations, as indicated in Figure 5.7. We have employed Walsh switching to minimize crosstalk to the extent possible. Assuming that most of the crosstalk occurs in the control room due to the close proximity of the I.F. cables and DC offsets in the A/D converters, as shown in the Figure 5.8, the output from each antenna base is passed through a phase switch immediately after they enter the control building. The latter is periodically inverted using orthogonal binary sequences. Since the switching period is an integer fraction of the integration period, the crosstalk signals get averaged to zero as they are correlated positively and negatively during the two halves of the integration period. The switching scheme used in the PBDA is

shown in the Figure 5.9. This phase inversion scheme is subsequently demodulated at the output of the sampler (see Ramesh, 1998 for details on the scheme).

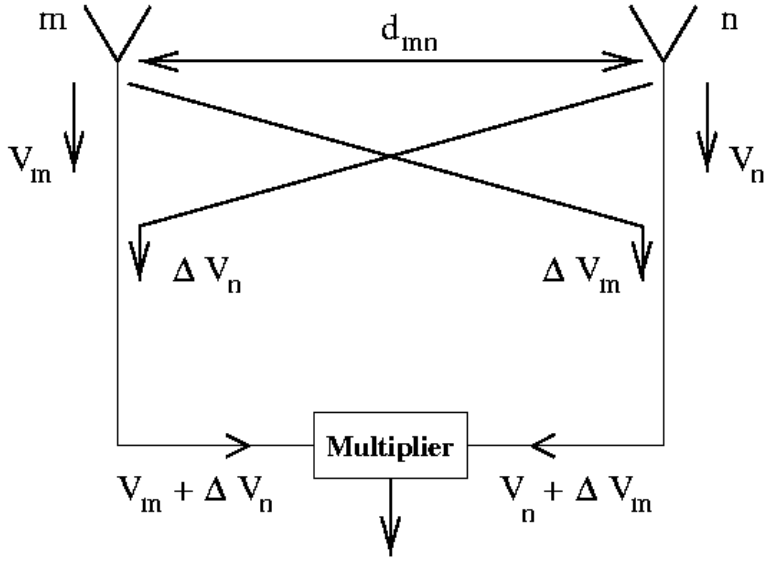

FIGURE 5.7 – Cross-talk in a two element interferometer.

5.4 - Digital delay system

The output of a correlation interferometer is given by (Thompson et al. 1994),

$$F = \cos\left(\frac{2\pi D\varepsilon\nu}{c}\right) \tag{5.2}$$

where D is the baseline length, $\varepsilon = \sin\theta$ is the direction cosine measured with respect to the baseline, ν is the frequency of observation and θ is the angle between the wavefront and the normal to the baseline. Note however, that the above expression is true only if the observing frequency is strictly monochromatic.

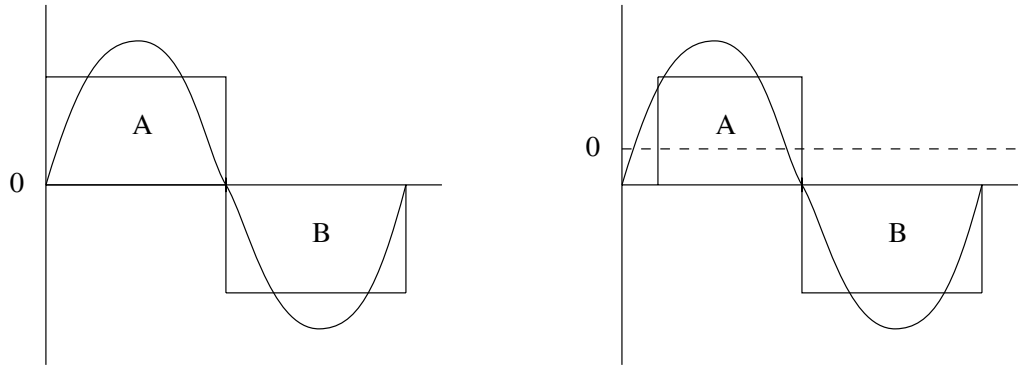

FIGURE 5.8 – DC offset in the A/D converter.

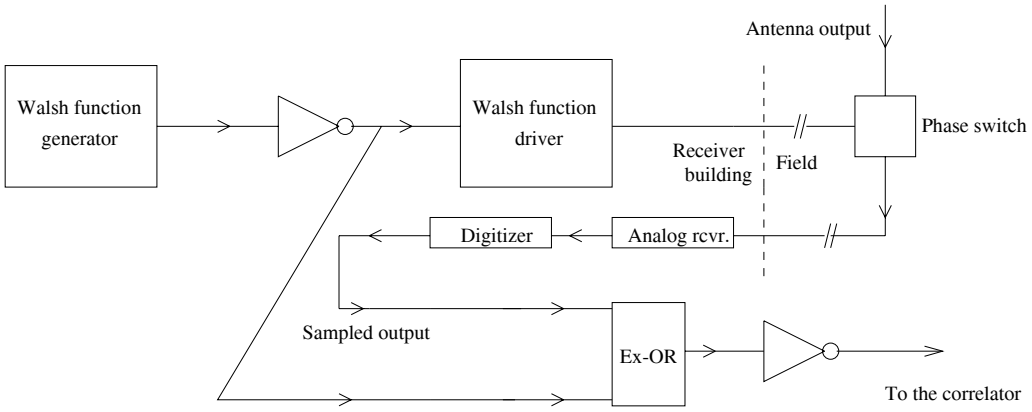

FIGURE 5.9 – Switching scheme used in the BDA.

In general the received signals are averaged over a rectangular band of width $\Delta\upsilon$ and center frequency υ_0. So, equation 5.2 becomes,

$$F(\nu_o) = -\frac{1}{\Delta\nu}\int_{\nu_o-\Delta\nu/2}^{\nu_o+\Delta\nu/2}\cos\left(\frac{2\pi D\varepsilon\nu}{c}\right) \tag{5.3}$$

$$F(\nu_o) = \cos\left(\frac{2\pi\varepsilon\nu_o}{c}\right)\frac{\sin(\pi D\varepsilon\Delta\nu/c)}{\pi D\varepsilon\Delta\nu/c} \tag{5.4}$$

Thus the output is modulated by a sinc function envelope which will be maximum only if the delay ($\tau = D\varepsilon/c$) between the two signals at the correlator input is zero. If the delay between the signals is not compensated before correlation, it will lead to a loss in the coherence between the two signals.

The modulating function in the equation 5.4 is also called the bandwidth de-correlation function or fringe-washing function. In view of the above, it is necessary to appropriately delay the signal reaching the two antennas of an interferometer (particularly for observations away from the zenith) to preserve coherence. In BDA, the above is accomplished by passing the signal through a delay unit (Figure 5.10) which can compensate the geometrical delay suffered by the signal in steps of 0.2 μs as mentioned earlier. Figure 5.11 shows solar observations carried out in the tracking mode with PBDA antennas 1 and 3 in the manner described above.

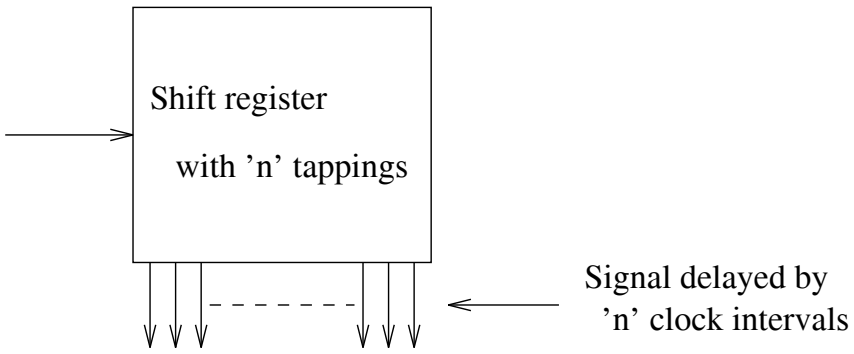

FIGURE 5.10 – Delay unit.

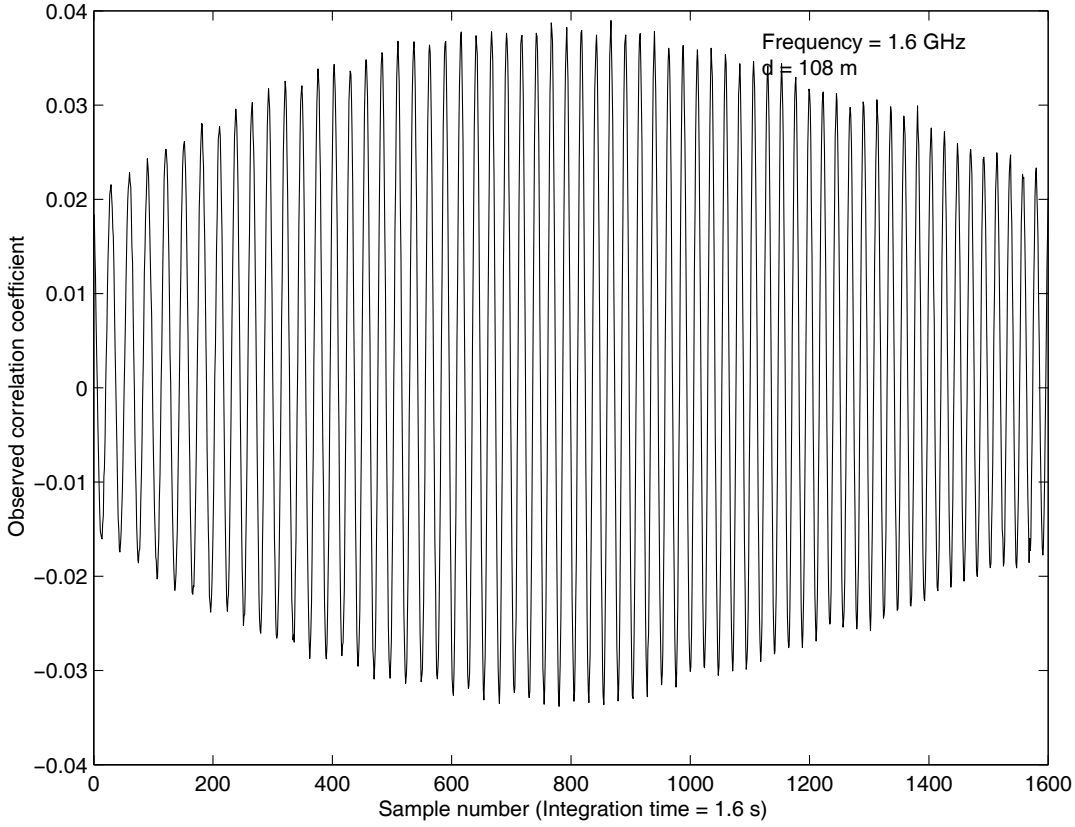

FIGURE 5.11 - Solar observations carried out with the PBDA antennas 1 and 3 in tracking mode on December 4, 2004.

6 - CONFIGURATION OF THE PBDA

6.1 - BDA configuration aspects

Radio interferometers, like the planned BDA, measure the Fourier transform of the radio sources, obtained from observations on a finite set of points in the Fourier plane. These points are determined by the cross-correlation of all possible pairs of antennas in the array (Wohlenben et al., 1991; Thompson et al., 1994). The image of a radio source can then be obtained by the inverse Fourier transform of the sampled data. Each pair measures a specific Fourier component given by the projected distance of the antenna in a plane that is normal to the incident angle of the radiation. Therefore, the sampling in the Fourier plane performed by the array is mainly dependent on the configuration. In addition, the physical layout of the array is very important to optimize the performance of the overall system.

Several approaches have been proposed to optimize the response of the array (Keto, 1997; Cornwell, 1988; Kogan, 2000). It is clear that the best array configuration is dependent on the scientific goals intended for the array. In generic interferometers, the best imaging performance is achieved when sampling in the Fourier domain is more uniform for a circular boundary defined by the spatial resolution of the array (Keto, 1997). This kind of sampling in the Fourier plane provides images less affected by errors caused by non-measured Fourier components. However, the optimization of the antenna positioning involves several others aspects that may be conflicting, such as cost or geographic constraints and requirements of the scientific goals.

The BDA is being designed to obtain optimized images of the radio sources at the decimetric band with high temporal and spatial resolutions. This precludes the use of Earth rotation synthesis (Thompson et al., 1994), requiring snapshot image acquisition. The BDA "T" shape configuration is suitable since it yields a uniform sampling in a rectangular region when using a regular spacing between antennas, not requiring the use of a gridding technique (Nakajima et al., 1994). Therefore, it requires less processing time In addition, this shape is good considering the site constraints as well as implementation and maintenance costs. In phase-I of the PBDA, a one-dimensional array of five elements was established with an aim to fulfill various diverse requirements. Specifically, the PBDA was used to accomplish some engineering tests in order to optimize the electronic subsystems of the PBDA for the following phases, as well as, to perform the first solar observations and obtain one-dimensional information about the brightness distribution of the Sun. The PBDA implemented at INPE in Cachoeira Paulista, São Paulo (Longitude 45º 0' 20" W, Latitude 22º 41' 19" S) has 5 antennas arranged along the E-W direction, operating in one-dimensional mode at frequency of 1.6 GHz with integration time of 100 ms. The largest baseline is 216 m and the minimal spacing between antennas is 18 m. This configuration has a spatial resolution of ~2.8 arc minutes at 1.6 GHz and a Field of View (FOV) of 40 arc minutes.

The option for implementing a one-dimensional array is suitable considering the limited number of antennas of the array. The PBDA has 5 antennas, this implies that there are 10 interferometric pairs (N*(N-1)/2), or in other words, 10 samples of the visibility function of the observed source. The implementation of a one-dimensional array allowed one to obtain uniform sampling of the uv plane and consequently, to provide images least susceptible to errors due unmeasured Fourier components. This one-dimensional configuration also permits the use of a maximum baseline of 216 m, which is important in the development of technology for transmission/reception radio signals for the long distances necessary for the development of the subsequent phases of the BDA. Figure 6.1 illustrates the configuration of the PBDA.

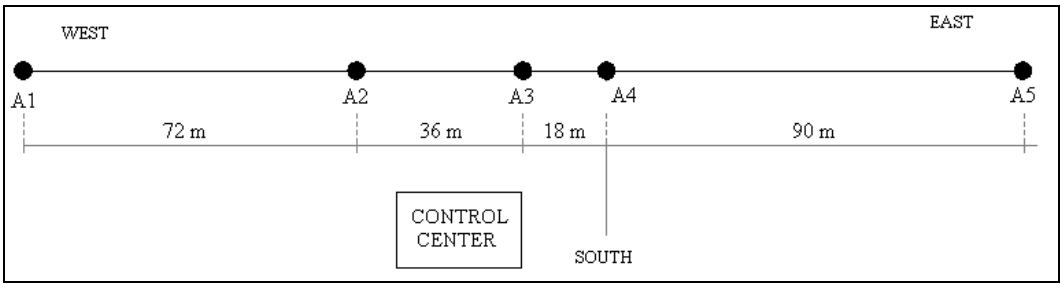

FIGURE 6.1 - PBDA array configuration (phase I).

Designating the West and East last antennas as A1 and A5, respectively, the spacing between the individual antennas (in terms of their multiplications) are given in Table 6.1.

TABLE 6.1 – Baseline lengths of the PBDA.

Antenna Multiplication	**Baseline (m)**
A1 × A2	72
A1 × A3	108
A1 × A4	126
A1 × A5	216
A2 × A3	36
A2 × A4	54
A2 × A5	144
A3 × A4	18
A3 × A5	108
A4 × A5	90

6.2 - UV coverage and beam of the PBDA

In order to simulate the performance of the PBDA, for radio imaging of the SUN, specific software was developed to simulate the data produced by PBDA observations. Its user interface was developed using the Interactive Data Language (IDL). This software allows one to choose the methodology for treatment of the radio interferometric data produced by the PBDA, as well as, to investigate possible configurations for the positioning of the BDA antennas.

The generation of simulated data of the BDA includes the following steps:

1. Performing of the Fourier transform of the source model using the FFT algorithm to obtain the discrete visibility function.
2. For each configuration, evaluating the sampling function in the Fourier plane (S), commonly named uv-coverage.
3. Sampling of the Fourier transform of the source model at the points defined by the sampling function *S*.
4. Inversion of the sampled visibilities obtaining the dirty image of the source (I^D).

The implementation of the procedures above in a computational system for simulation of the images generated for the BDA allows one to study the effect of each array configuration in the uv-plane and the consequent quality of the synthesized image. A graphical interface allows

the user to choose the number of antennas to be used, as well as, its localization in the plane of the array. From a chosen configuration, it is possible to compute the sampling function of the array that is used to sample the visibility function of the model of the source. Applying the inverse Fourier transform to this sampled visibility function yields the synthesized image (dirty image). The use of image restoration techniques allows one to estimate the original brightness distribution of the source from the dirty image. In radio astronomy, the restoration process has been mainly dominated by two classic algorithms: the Maximum Entropy Method (MEM) (Jaynes, 1957; Narayan and Nityananda, 1986) and the CLEAN algorithm (Hogbom, 1974; Clark, 1980).

During the PBDA, investigations of the imaging capabilities of its configuration were carried out. The uv-coverage and the dirty beam of the PBDA are shown in Figure 6.2. Table 6.2 shows the main parameters used in the simulation.

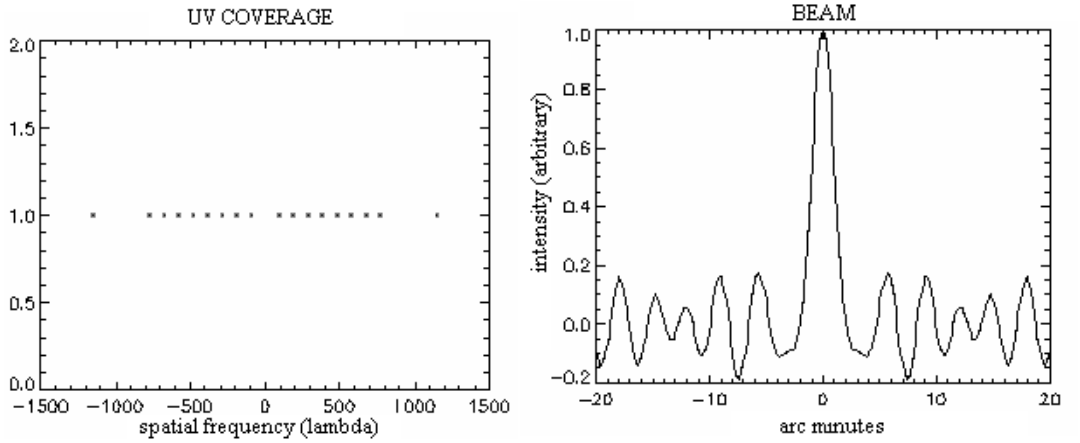

FIGURE 6.2 – UV coverage and synthesized beam of PBDA.

TABLE 6.2 – Parameters of the BDA data simulation.

Antennas positions: -90 0 18 54 126
Wavelength (m): 0.187559
Field of View (arc minutes): 40
Spatial resolution (arcmin): 2.98509
baselines (m): 18 36 54 72 90 108 108 126 144 216

6.3 - Expected spatial resolution

The PBDA will obtain the complex visibilities for all the interferometric pairs of antennas shown in Figure 6.3.

A1×A2
A1×A3 A2×A3
A1×A4 A2×A4 A3×A4
A1×A5 A2×A5 A3×A5 A4×A5

FIGURE 6.3 - Correlations performed by PBDA correlator system.

The digital correlation system of the BDA performs correlations for all pairs of antennas, producing 20 measurements of the visibility function of the celestial source. These measurements correspond to the cosine and sine channels of the 10 complex correlator pairs, with integration time of 100 ms. The beam width is approximately 1/10 of the solar disc (~2.8 arc minutes for baseline A1×A5 at 1.6 GHz).

The spatial resolution of an interferometer is given by:

$$\delta = \sin^{-1}(\lambda / B) \tag{6.1}$$

where λ is the observed wavelength and B is the distance between the antennas that compose an interferometric pair. Table 6.3 shows the expected spatial resolution for all baselines of the PBDA.

TABLE 6.3 - Baselines and expected resolution for the PBDA at 1.6 GHz.

ANTENNA MULTIPLICATION	EXPECTED SPATIAL RESOLUTION (arc minutes)
A1 × A2	35.8
A1 × A3	17.9
A1 × A4	11.9
A1 × A5	8.95
A2 × A3	7.16
A2 × A4	5.96
A2 × A5	5.11
A3 × A4	4.47
A3 × A5	2.98

The control building (Figure 6.1) is located at about 30 meters from the center of the array. Control and acquisition of the PBDA data are performed by computers located at this building. The data acquisition system, developed by the Indian Institute of Astrophysics (IIA), is responsible for acquiring the output of the complex correlators for all interferometric pairs. The measured visibility data is stored in ASCII files for further processing. Imaging software, developed in IDL, performs the synthesis of BDA images. During PBDA development the first astronomical observations were made with the antennas running in transit mode. The observed fringes were obtained using the software described above and it was possible to obtain a one-dimensional profile of the Sun.

6.3.1 - Observed spatial resolution

The observed spatial resolution of all baselines was obtained from the fringes given by the digital correlator system during observation of the Solar transit. Section 6.4.3 presents a catalogue with the sine and cosine fringes obtained for all the BDA baselines in the observations of the solar transit in December 11th of 2004. It was possible, by means of these fringes, to measure the spatial resolution of each baseline of the array in order to compare the expected and the observed resolution. The observed spatial resolution of each baseline can be measured as the angular distance between two consecutive minima of the fringes for the corresponding interferometric pair. Table 6.4 presents the expected and the observed spatial resolution for all baselines of PBDA.

TABLE 6.4 - Baseline separation, expected and measured resolutions at 1.6 GHz for PBDA at INPE-CP.

ANTENNA MULTIPLICATION (CORRELATIONS)	BASELINE (m)	SPATIAL RESOLUTION (minutes of arc)	
		MEASURED	EXPECTED
A1 × A2	18	36.4	35.8
A1 × A3	36	18.2	17.9
A1 × A4	54	12.2	11.9
A1 × A5	72	9.05	8.95
A2 × A3	90	7.26	7.16
A2 × A4	108	6.10	5.96
A2 × A5	126	5.20	5.11
A3 × A4	144	4.61	4.47
A3 × A5	216	3.02	2.98

6.4 - Calibration Scheme for the PBDA

A two-element correlation interferometer measures the spatial coherence of a distant radiation field at a given location as a function of the separation between the antennas, or baseline, measured in wavelengths. The output is usually referred as the visibility function and is denoted by V_{ij}, with the sub-scripts indicating which pair of antennas is involved. An array of antennas samples this visibility function at many discrete locations. The process of calibration recovers the true visibilities from the observed quantities which are often corrupted for a multitude of reasons. Due to these errors the observed complex visibility (V^{obs}) on a certain baseline differs from the true response (V^{true}) leading to inaccuracies in the determination of the sky brightness distribution. The measured visibility on the baseline formed by the antennas G_i and G_j can be written as:

$$V_{ij}^{obs} = V_{ij}^{true} g_i g_j^* g_{ij} + c_{ij} + \varepsilon_{ij} \qquad (6.2)$$

Here g_i & g_j are the total complex gains for i^{th} and j^{th} antenna (incorporating all the antenna based amplitude and phase errors. * in the above equation denotes complex conjugation). The term g_{ij} represents the baseline dependent complex gain; c_{ij} is an additive error consisting of e.g., correlator offsets and ε_{ij} is the thermal noise plus possible interference.

6.4.1 - Amplitude calibration

We had planned to use observations of the following sources:

1) Virgo A (3C274 or M87), S 1600 ≈ 166 Jy
   RA (2004.1) = $12^h\ 31^m\ 05^s$, Dec (2004.1) = $12^o22'$,
2) Taurus A (3C144 or M1), S_{1600} ≈ 897 Jy
   RA (2004.1) = $05^h\ 34^m\ 48^s$, Dec (2004.1) = $22^o00'$, and
3) Cygnus A (3C405), S_{1600} ≈ 1257 Jy
   RA (2004.1) = $19^h\ 59^m\ 39^s$, Dec (2004.1) = $40^o\ 45'$

for calibrating the visibility amplitude obtained from Sun (target source) on each baseline. But we could obtain data on the above calibrator sources only on three baselines (1 × 2, 1 × 3 and 2

x 3) due to pointing error in the antennas 4 and 5. Note that the above error should be very minimal particularly for observations on a calibrator source since its angular size will be usually much smaller compared to the primary beam of the individual antennas. The half-power beam width (HPBW) of the antennas used in the PBDA is $\approx 2.5^{\circ}$ at 1.6 GHz. To overcome this problem, we assumed that there is no gain variation between the different channels in both the analog and digital receiver systems, and calibrated the amplitude of the solar data on all the baselines using the calibrator data on the above three baselines. However, before carrying out the above step, we independently checked the receiver system for possible gain variations by performing a 'noise' test. The deviations were found to be very small. Again, we maintained the input to the different channels at the same level. Inspite of this, still there could be some error. But, we do know its magnitude at this stage. It may not be significant since the BDA digital correlator system uses 1-bit, 2-level sampling where the input signal is clipped and the absolute strength information is lost. We separately measure the total power received by the individual antennas to obtain the latter (see Ramesh, 1998, Ramesh et al., 1998, Ramesh et al, 1999 for more details).

6.4.2 - Phase calibration

Neglecting the errors due to noise in the receiver system, the phase of the observed complex visibility on the baseline formed by the antenna groups G_i and G_j is given by,

$$\phi_{ij}^{obs} = \phi_{ij}^{true} + \phi_i^{err} - \phi_j^{err} \tag{6.3}$$

where $\phi_{\mathrm{i}}^{\mathrm{err}}$ & ϕ_j^{err} are the phase of the i^{th} & j^{th} antennas (with respect to an arbitrary reference point) and ϕ_{ij}^{g} is the geometric phase term (due to the orientation of the interferometer baseline with respect to the direction of the source). Jennison (1958) first showed that the antenna based errors ($\phi_{\mathrm{i}}^{\mathrm{err}}$, ϕ_j^{err}) can be effectively eliminated from the above equation by forming a closure relation between the antenna groups G_i , G_j and G_k as shown below.

$$\phi_{ijk} = \phi_{ij}^{obs} + \phi_{jk}^{obs} - \phi_{ik}^{obs} \tag{6.4}$$

i.e.,

$$\phi_{ijk} = \phi_{ij}^{true} + \phi_{jk}^{true} - \phi_{ik}^{true} \tag{6.5}$$

This equation is free of any error terms. By forming all possible closure equations of this type in an N element interferometer and arranging them in the matrix form,

$$Ax = b \tag{6.6}$$

where, A - coefficient matrix; x - column matrix consisting of the $\left(\phi^{true}\right)^s$ and b - column matrix consisting of the closure phases, i.e. ϕ^s

One can solve for the true visibility phase $\left(\phi^{true}\right)$ on any baseline using matrix inversion techniques. These phases can then be combined with the observed amplitudes on the corresponding baseline to form the true complex visibility pertaining to the source (see also Rogstad, 1968; Readhead and Wilkinson, 1978; Pearson and Readhead, 1984 for details on closure quantities).

6.4.3 - Application of BDA

Consider the multiplications between the antennas G_1 ; G_2 ; G_3 ; G_4 and G_5. The closure equations are,

$$\phi_{1,2,3} = \phi_{1,2}^{true} + \phi_{2,3}^{true} - \phi_{1,3}^{true}$$

$$\phi_{1,2,4} = \phi_{1,2}^{true} + \phi_{2,4}^{true} - \phi_{1,4}^{true}$$

$$\phi_{1,2,5} = \phi_{1,2}^{true} + \phi_{2,5}^{true} - \phi_{1,5}^{true}$$

$$\phi_{1,3,4} = \phi_{1,3}^{true} + \phi_{3,4}^{true} - \phi_{1,4}^{true}$$

$$\phi_{1,3,5} = \phi_{1,3}^{true} + \phi_{3,5}^{true} - \phi_{1,5}^{true}$$

$$\phi_{1,4,5} = \phi_{1,4}^{true} + \phi_{4,5}^{true} - \phi_{1,5}^{true}$$

$$\phi_{2,3,4} = \phi_{2,3}^{true} + \phi_{3,4}^{true} - \phi_{2,4}^{true}$$

$$\phi_{2,3,5} = \phi_{2,3}^{true} + \phi_{3,5}^{true} - \phi_{2,5}^{true}$$

$$\phi_{2,4,5} = \phi_{2,4}^{true} + \phi_{4,5}^{true} - \phi_{2,5}^{true}$$

$$\phi_{3,4,5} = \phi_{3,4}^{true} + \phi_{4,5}^{true} - \phi_{3,5}^{true} \qquad (6.7)$$

There are 10 equations; whereas the unknowns (ϕ_{ij}^{true}) to be solved for are only 9 (the multiplications 1×3 and 3×5 measure the same visibility). But for all practical purposes, we treat them independent and solve for all the 10 unknowns. This problem can be better understood if the above set of equations is written in a matrix form as shown below:

$$\begin{pmatrix} 1 & -1 & 0 & 0 & 1 & 0 & 0 & 0 & 0 & 0 \\ 1 & 0 & -1 & 0 & 0 & 1 & 0 & 0 & 0 & 0 \\ 1 & 0 & 0 & -1 & 0 & 0 & 1 & 0 & 0 & 0 \\ 0 & 1 & -1 & 0 & 0 & 0 & 0 & 1 & 0 & 0 \\ 0 & 1 & 0 & -1 & 0 & 0 & 0 & 0 & 1 & 0 \\ 0 & 0 & 1 & -1 & 0 & 0 & 0 & 0 & 0 & 1 \\ 0 & 0 & 0 & 0 & 1 & -1 & 0 & 1 & 0 & 0 \\ 0 & 0 & 0 & 0 & 1 & 0 & -1 & 0 & 1 & 0 \\ 0 & 0 & 0 & 0 & 0 & 1 & -1 & 0 & 0 & 1 \\ 0 & 0 & 0 & 0 & 0 & 0 & 0 & 1 & -1 & 1 \end{pmatrix} \begin{pmatrix} \phi_{1,2}^{true} \\ \phi_{1,3}^{true} \\ \phi_{1,4}^{true} \\ \phi_{1,5}^{true} \\ \phi_{2,3}^{true} \\ \phi_{2,4}^{true} \\ \phi_{2,5}^{true} \\ \phi_{3,4}^{true} \\ \phi_{3,5}^{true} \\ \phi_{4,5}^{true} \end{pmatrix} = \begin{pmatrix} \phi_{1,2,3} \\ \phi_{1,2,4} \\ \phi_{1,2,5} \\ \phi_{1,3,4} \\ \phi_{1,3,5} \\ \phi_{1,4,5} \\ \phi_{2,3,4} \\ \phi_{2,3,5} \\ \phi_{2,4,5} \\ \phi_{3,4,5} \end{pmatrix} \qquad (6.8)$$

Using the technique of singular value decomposition (SVD) to invert the coefficient matrix, a least squares solution (Press et al., 1992) for the true visibility phases are obtained. The latter are then combined with the corrected visibility amplitude, Fourier inverted and CLEANed (Hogbom, 1974) to obtain the one-dimensional brightness distribution (see Ramesh, 1998, Ramesh et al., 1998, Ramesh et al., 1999 for more details). We cross-checked the visibility phases obtained using the above technique for the multiplications 1×2, 1×3 and 2×3 with that obtained through the conventional method (i.e. correction of the phase error on individual baselines through observations of a calibrator source). The values agree well with each other. We make use of the phases obtained using the conventional method to fix the position of the source in the sky. Note that the latter will be lost when we use closure phase technique.

The one-dimensional brightness distribution of Sun obtained using the above method at 15:00 UT and 17:00 UT on December 11, 2004 is shown in Figures 6.4 and 6.5. The latter is compared with the 195 Å image of the solar corona obtained around the same time with the Extreme ultra-violet Imaging Telescope (EIT; Brueckner et al., 1995) onboard the Solar and Heliospheric Observatory (SoHO), (Fleck et al., 1995) to establish the correspondence between them (Figures 6.6 and 6.7). The following figures (6.8-6.37) show the fringes observed on different baselines for Cygnus A (Figures 6.8 - 6.13), Taurus A (Figures 6.14 - 6.19) and Sun (Figures 6.20 - 6.37) on December 10 and 11, 2004 at 1.6 GHz. The integration time used is 1.6 s for the Sun.

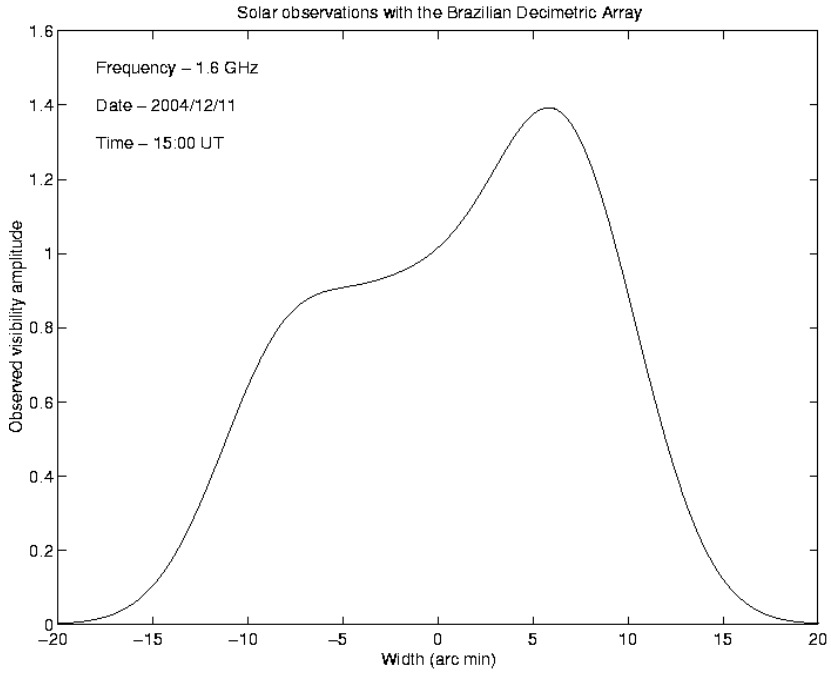

FIGURE 6.4 – The one-dimensional brightness distribution of Sun obtained with BDA at 15:00 UT on December 11, 2004.

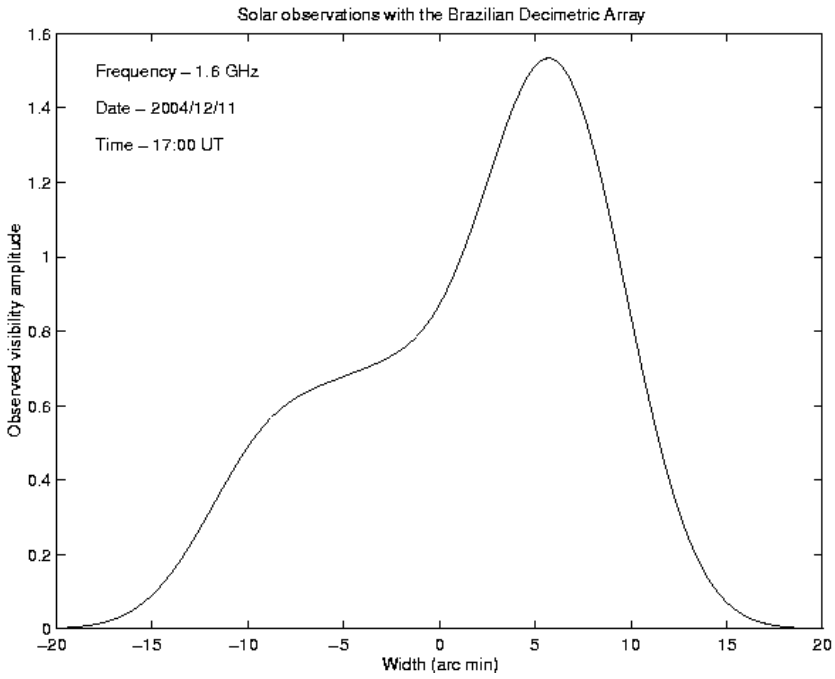

FIGURE 6.5 – The one-dimensional brightness distribution of Sun obtained with BDA at 17:00 UT on December 11, 2004.

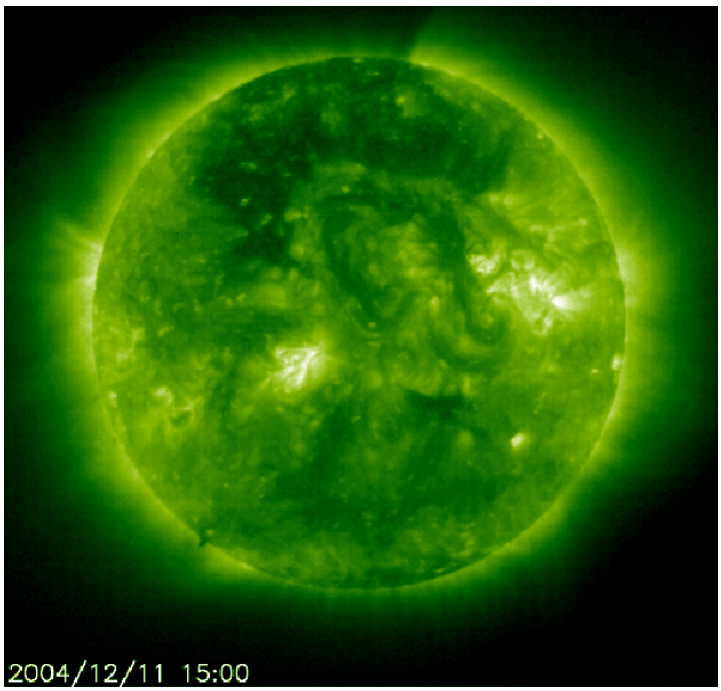

FIGURE 6.6 – A 195 Å image of the solar corona obtained on December 11, 2004 at 15:00 UT with the Extreme ultra-violet Imaging Telescope onboard the Solar and Heliospheric Observatory (SoHO).

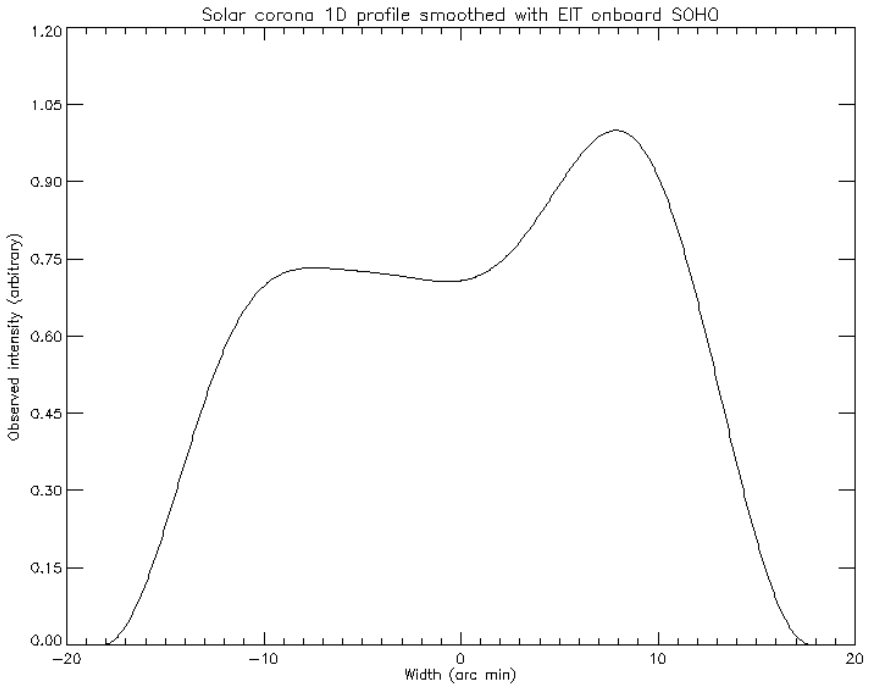

FIGURE 6.7 – The one-dimensional brightness distribution of the Sun obtained using SOHO satellite observations. The image of the Figure 6.6 was integrated in N-S of the Sun and smoothing in E–W direction by applying filter equivalent of beam of PBDA.

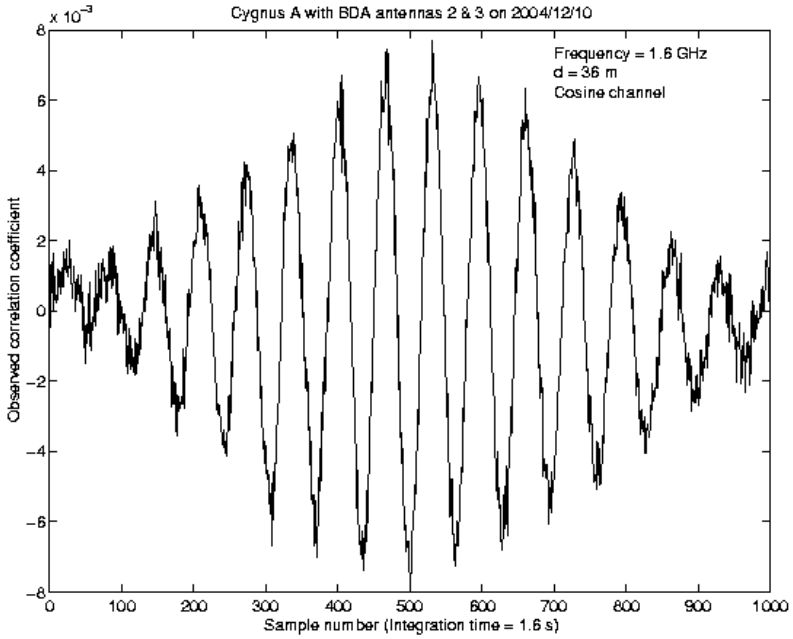

FIGURE 6.8 – Cosine Fringe obtained on 10/12/2004 throughout the interferometer pair composed of A2 and A3 antennas in the Cygnus A observation.

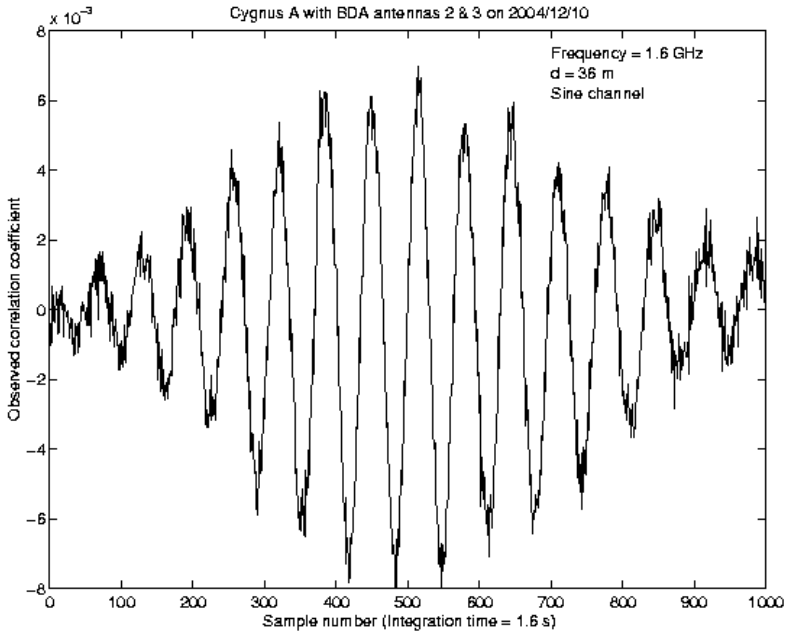

FIGURE 6.9 – Sine Fringe obtained on 10/12/2004 throughout the interferometer pair composed of A2 and A3 antennas in the Cygnus A observation.

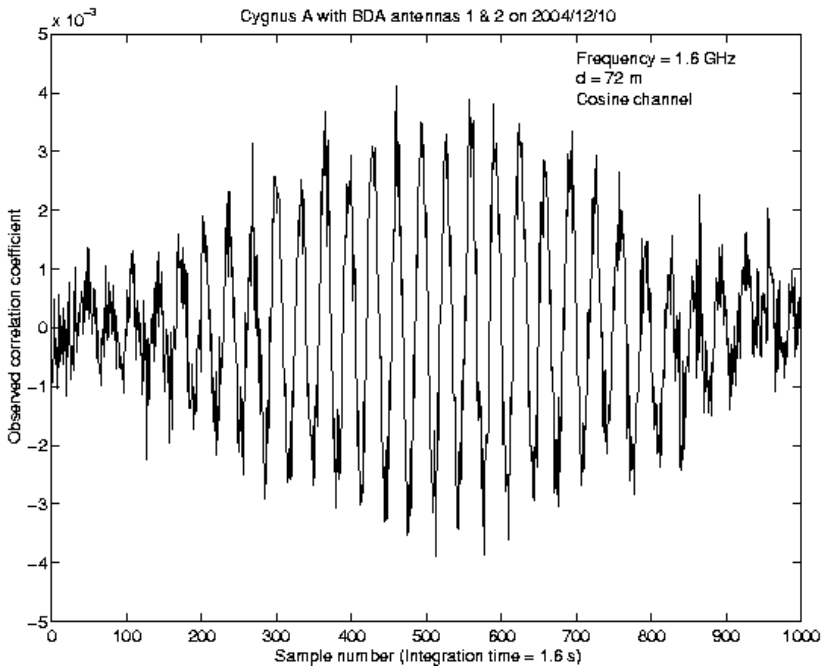

FIGURE 6.10 – Cosine Fringe obtained on 10/12/2004 throughout the interferometer pair composed of A1 and A2 antennas in the Cygnus A observation.

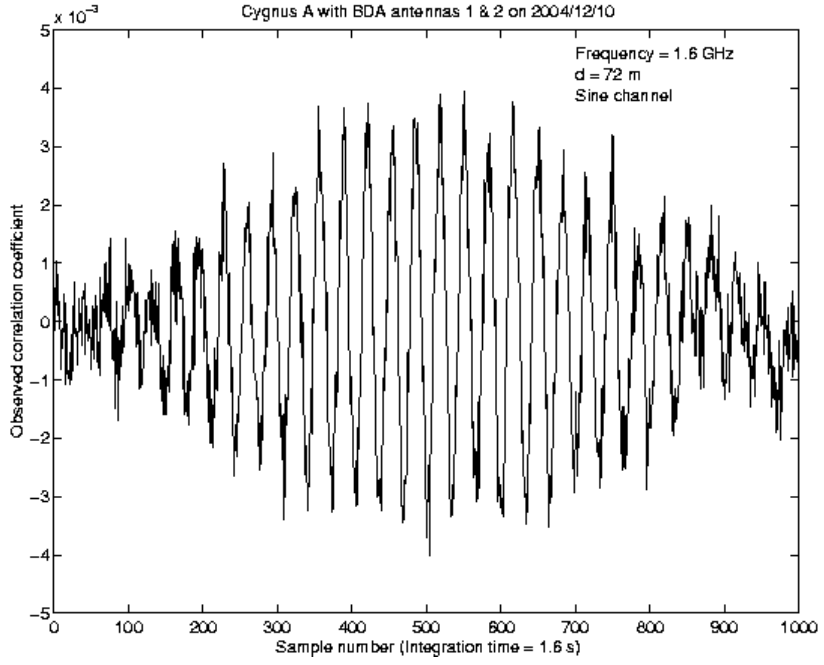

FIGURE 6.11 – Sine Fringe obtained on 10/12/2004 throughout the interferometer pair composed of A1 and A2 antennas in the Cygnus A observation.

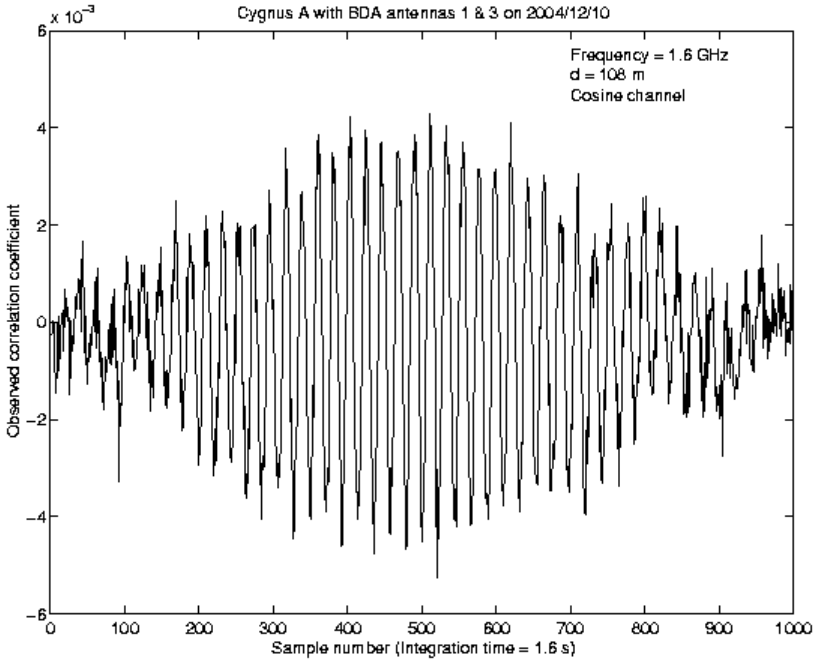

FIGURE 6.12 – Cosine Fringe obtained on 10/12/2004 throughout the interferometer pair composed of A1 and A3 antennas in the Cygnus A observation.

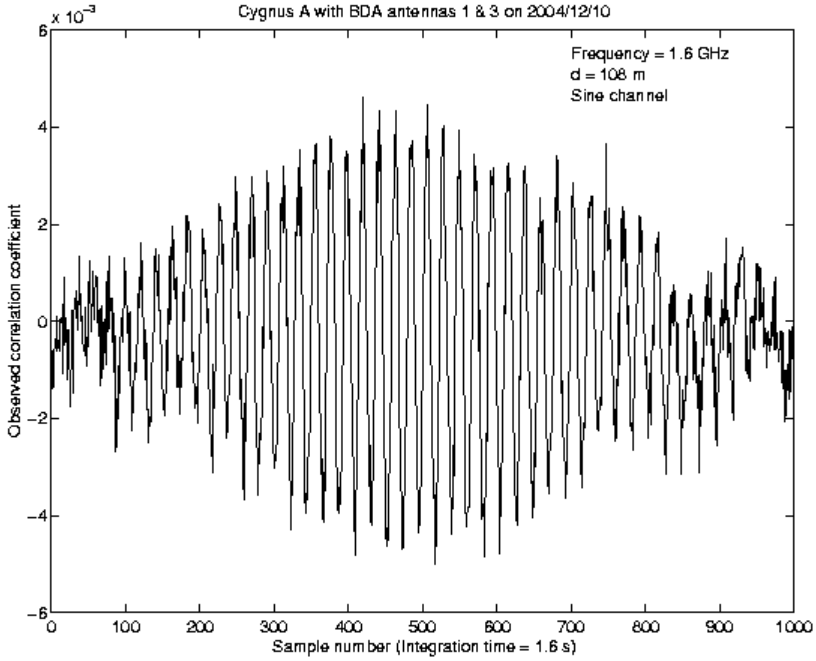

FIGURE 6.13 – Sine Fringe obtained on 10/12/2004 throughout the interferometer pair composed of A1 and A3 antennas in the Cygnus A observation.

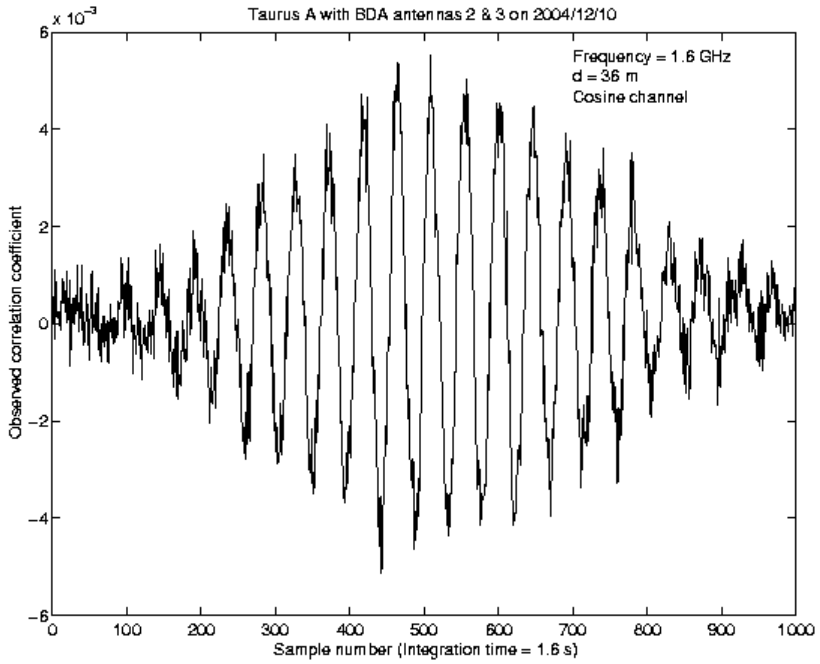

FIGURE 6.14 – Cosine Fringe obtained on 10/12/2004 throughout the interferometer pair composed of A2 and A3 antennas in the Taurus A observation.

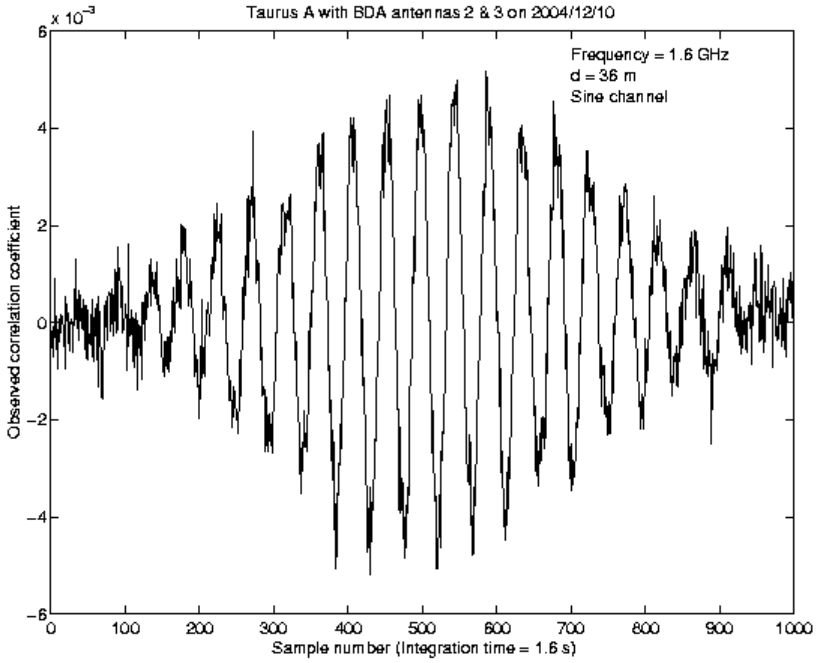

FIGURE 6.15 – Sine Fringe obtained on 10/12/2004 throughout the interferometer pair composed of A2 and A3 antennas in the Taurus A observation.

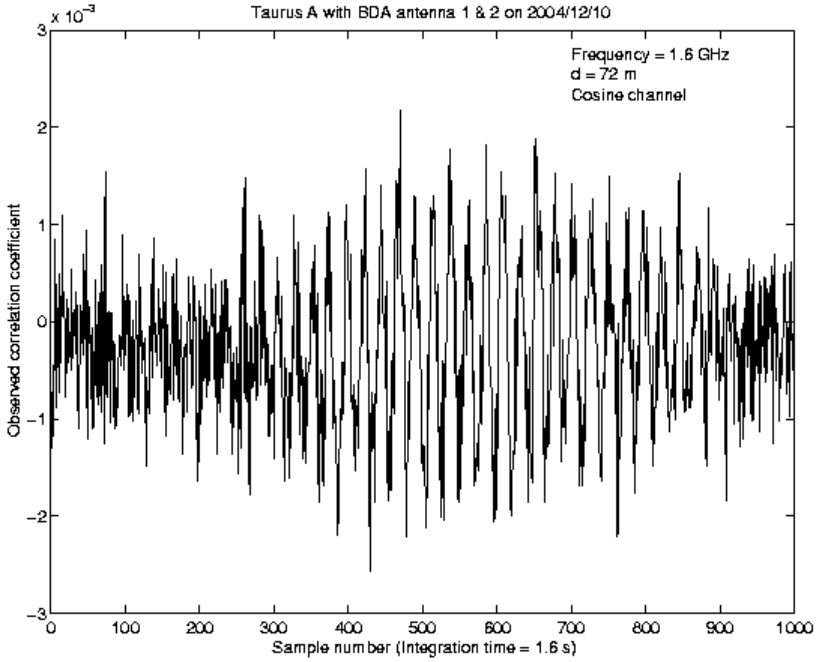

FIGURE 6.16 – Cosine Fringe obtained on 10/12/2004 throughout the interferometer pair composed of A1 and A2 antennas in the Taurus A observation.

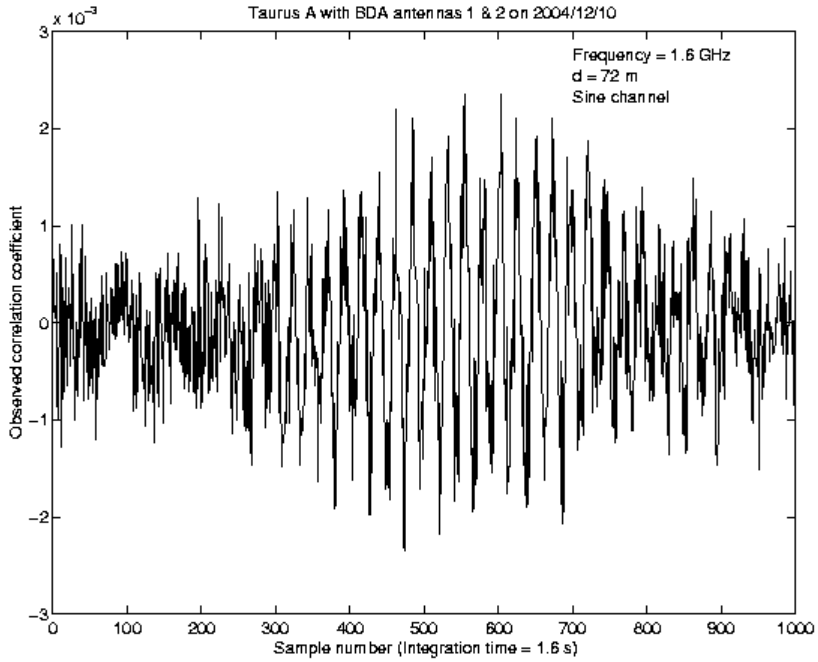

FIGURE 6.17 – Sine Fringe obtained on 10/12/2004 throughout the interferometer pair composed of A1 and A2 antennas in the Taurus A observation.

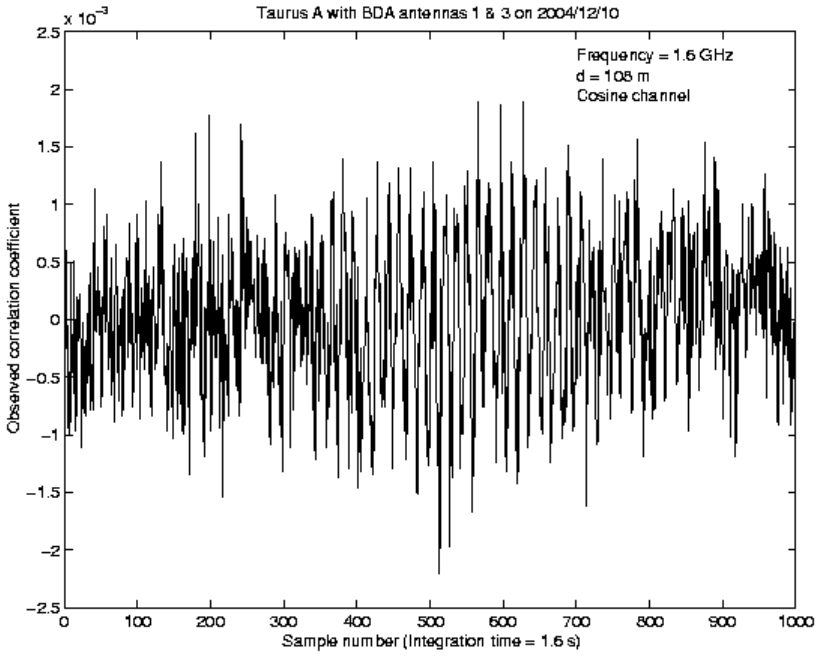

FIGURE 6.18 – Cosine Fringe obtained on 10/12/2004 throughout the interferometer pair composed of A1 and A3 antennas in the Taurus A observation.

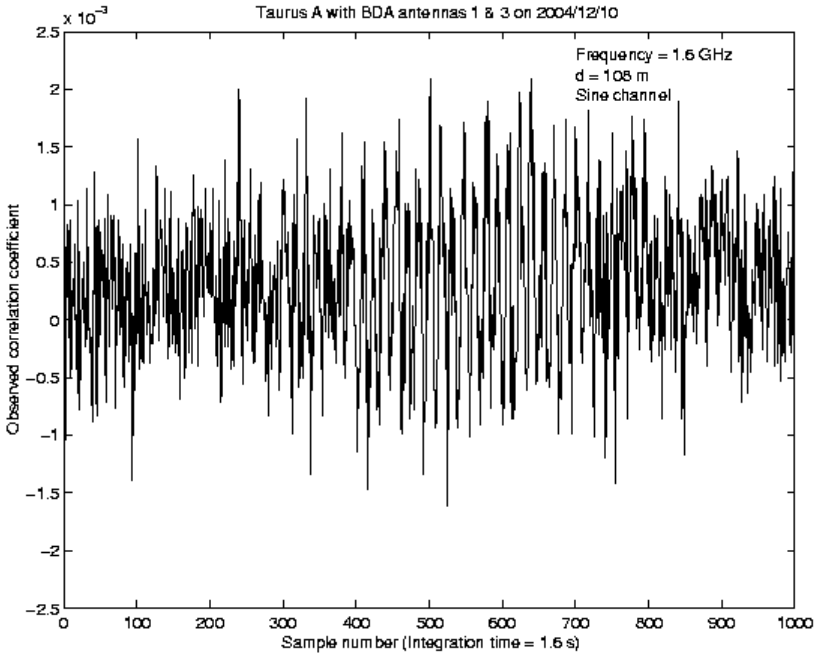

FIGURE 6.19 – Sine Fringe obtained on 10/12/2004 throughout the interferometer pair composed of A1 and A3 antennas in the Taurus A observation.

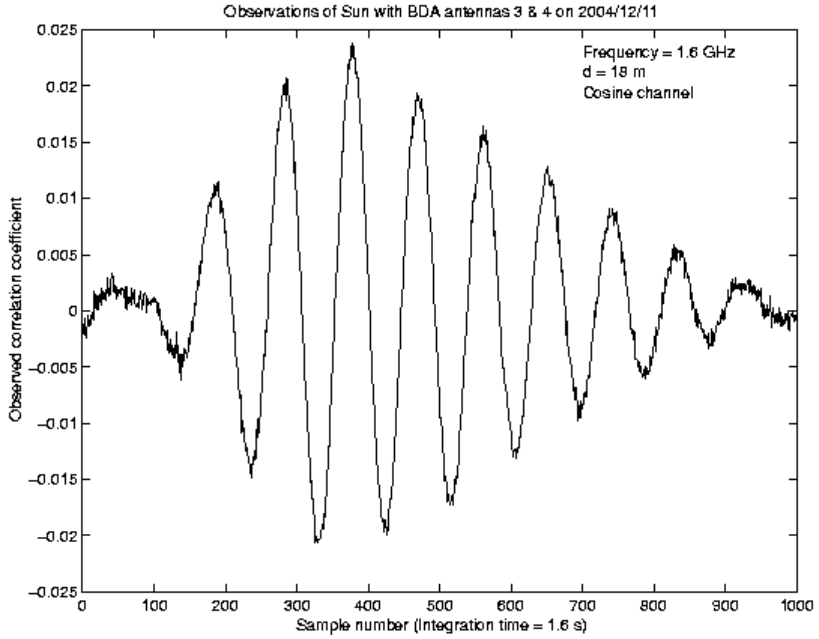

FIGURE 6.20 – Cosine Fringe obtained on 11/12/2004 throughout the interferometer pair composed of A3 and A4 antennas in the observation of Sun.

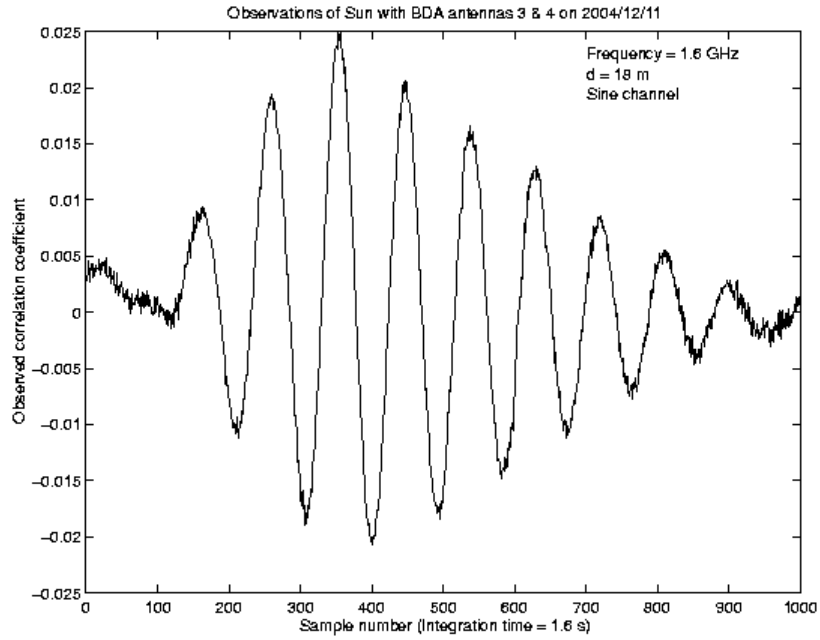

FIGURE 6.21 – Sine Fringe obtained on 11/12/2004 throughout the interferometer pair composed of A3 and A4 antennas in the observation of Sun.

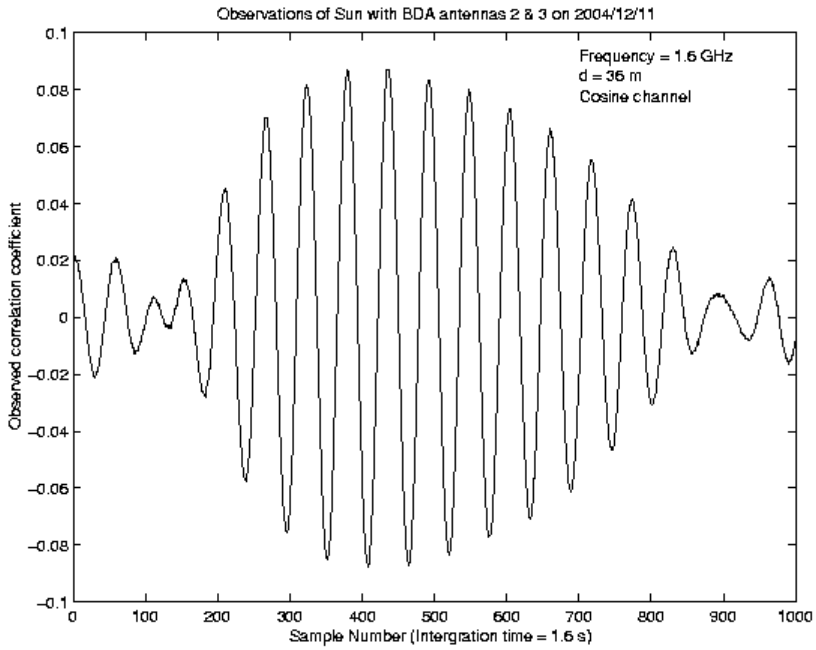

FIGURE 6.22 – Cosine Fringe obtained on 11/12/2004 throughout the interferometer pair composed of A2 and A3 antennas in the observation of Sun.

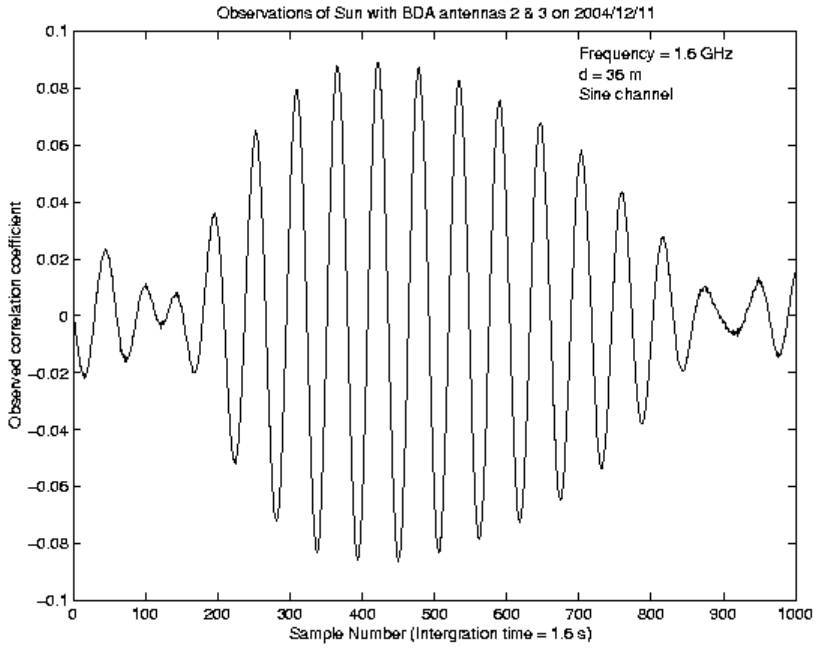

FIGURE 6.23 – Sine fringe obtained on 11/12/2004 throughout the interferometer pair composed of A2 and A3 antennas in the observation of Sun.

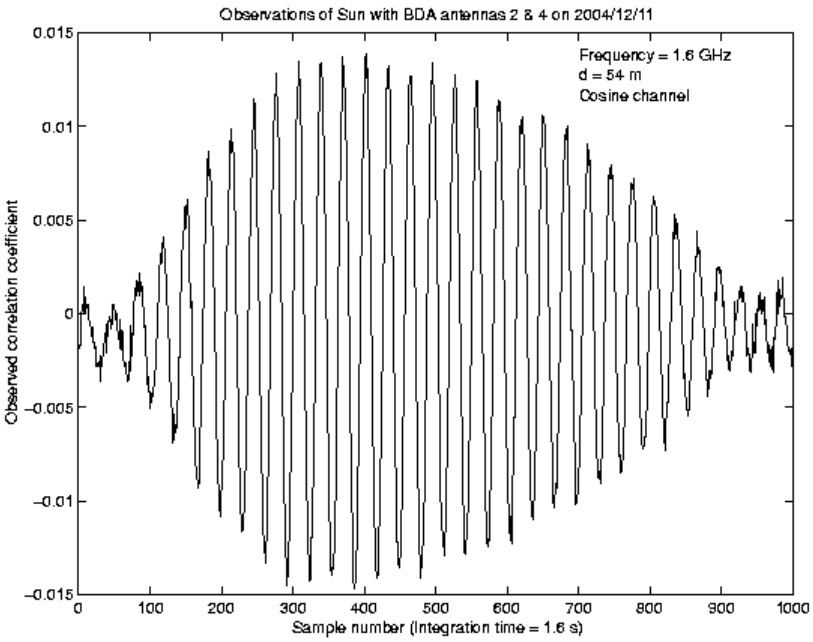

FIGURE 6.24 – Cosine fringe obtained on 11/12/2004 throughout the interferometer pair composed of A2 and A4 antennas in the observation of Sun.

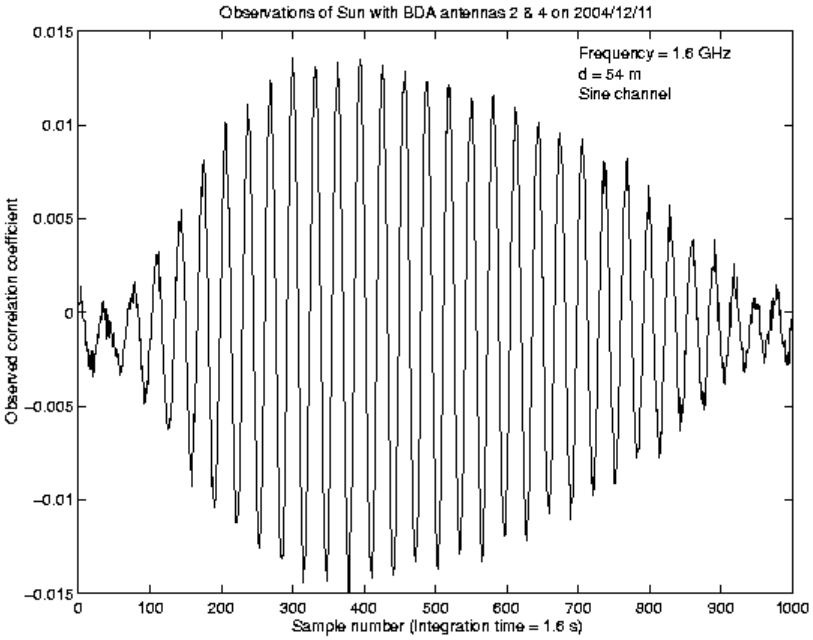

FIGURE 6.25 – Sine fringe obtained on 11/12/2004 throughout the interferometer pair composed of A2 and A4 antennas in the observation of Sun.

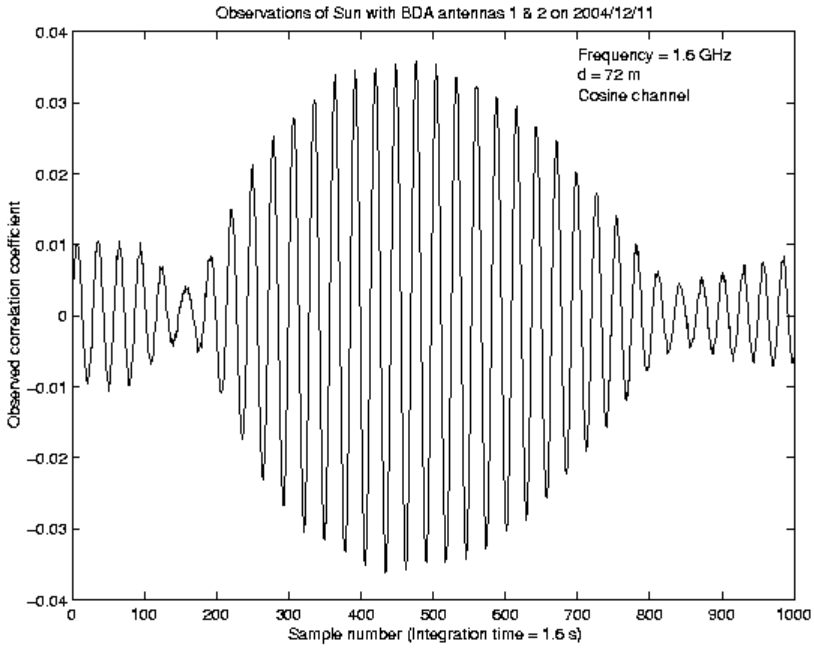

FIGURE 6.26 – Cosine fringe obtained on 11/12/2004 throughout the interferometer pair composed of A1 and A2 antennas in the observation of Sun.

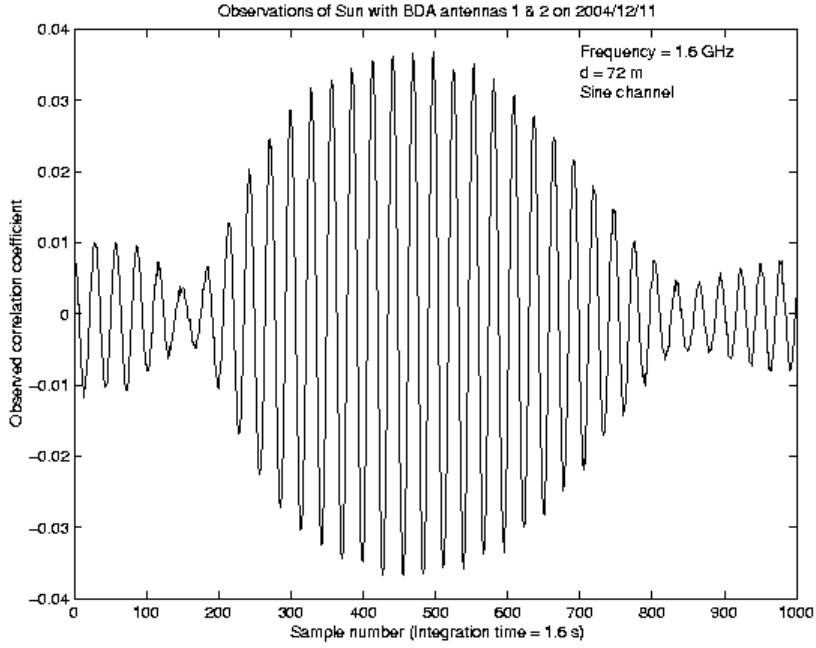

FIGURE 6.27 – Sine fringe obtained on 11/12/2004 throughout the interferometer pair composed of A1 and A2 antennas in the observation of Sun.

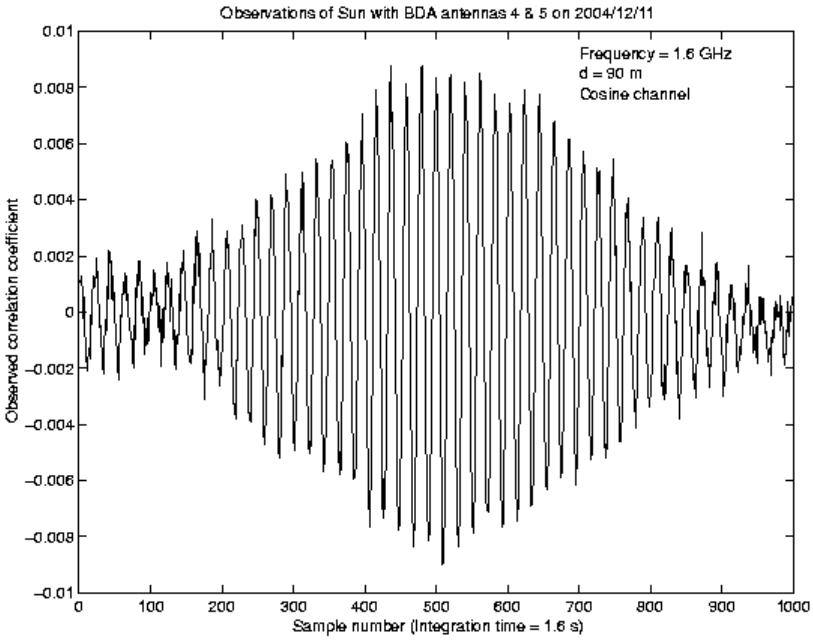

FIGURE 6.28 – Cosine fringe obtained on 11/12/2004 throughout the interferometer pair composed of A4 and A5 antennas in the observation of Sun.

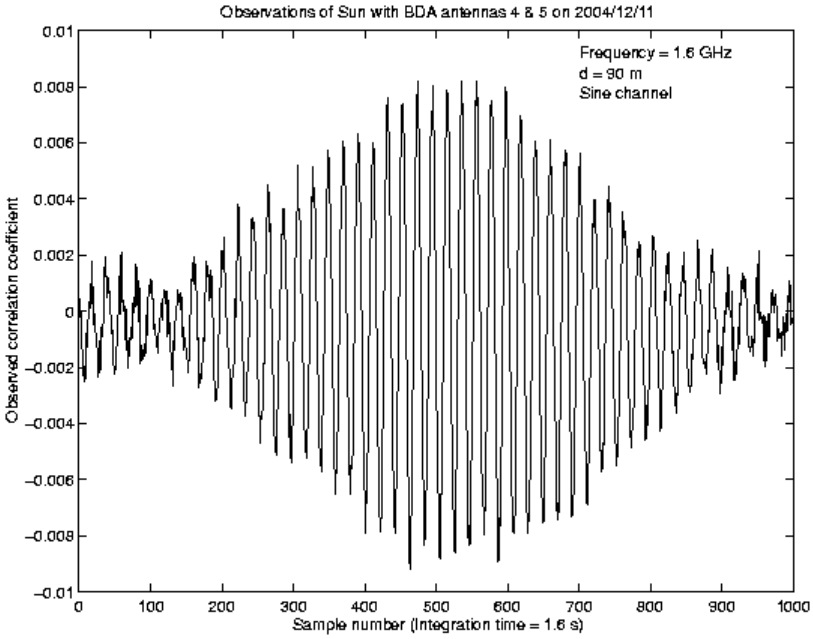

FIGURE 6.29 – Cosine fringe obtained on 11/12/2004 throughout the interferometer pair composed of A4 and A5 antennas in the observation of Sun.

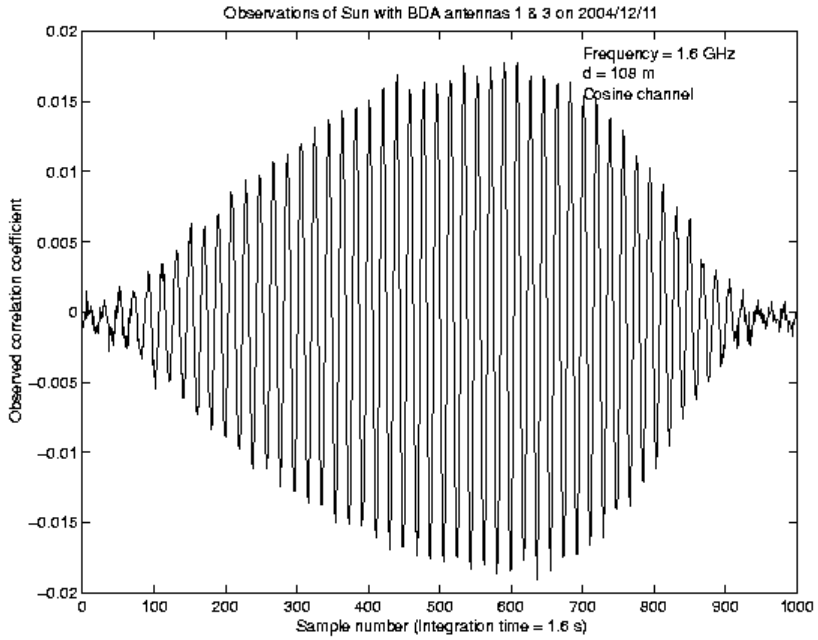

FIGURE 6.30 – Cosine fringe obtained on 11/12/2004 throughout the interferometer pair composed of A1 and A3 antennas in the observation of Sun.

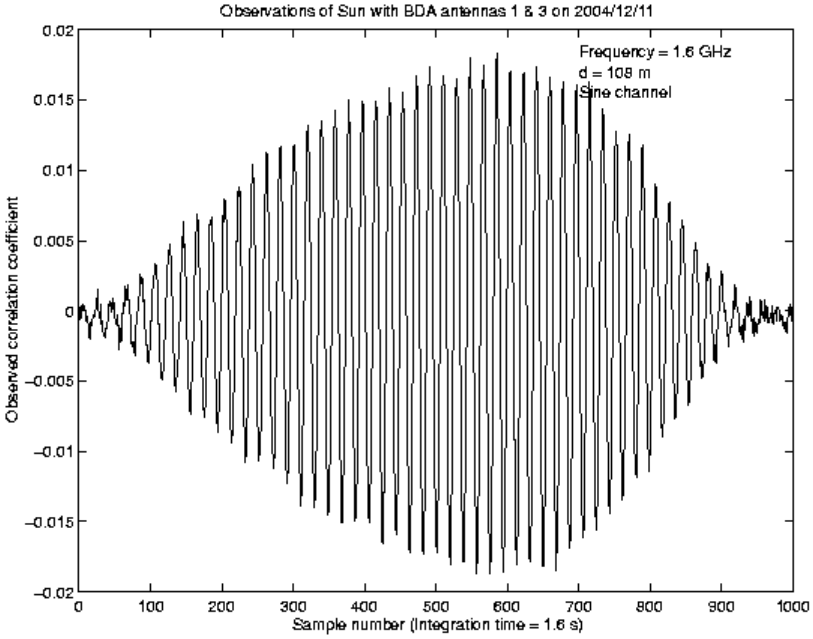

FIGURE 6.31 – Sine fringe obtained on 11/12/2004 throughout the interferometer pair composed of A1 and A3 antennas in the observation of Sun.

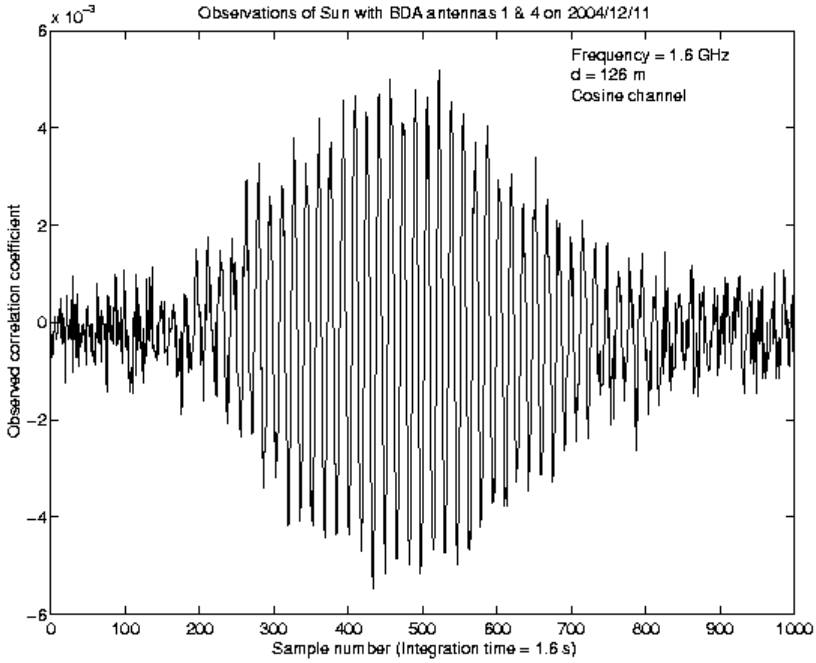

FIGURE 6.32 – Cosine fringe obtained on 11/12/2004 throughout the interferometer pair composed of A1 and A4 antennas in the observation of Sun.

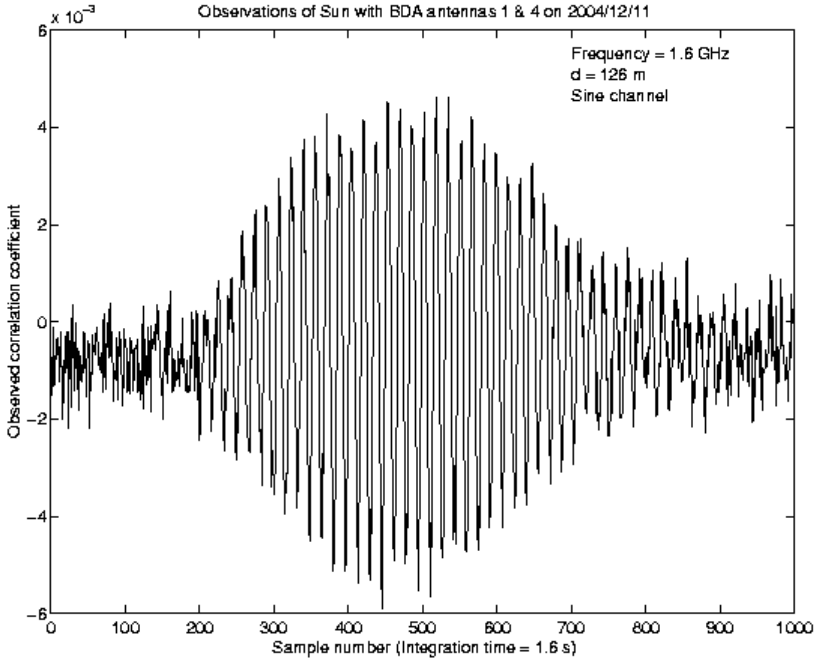

FIGURE 6.33 – Sine fringe obtained on 11/12/2004 throughout the interferometer pair composed of A1 and A4 antennas in the observation of Sun.

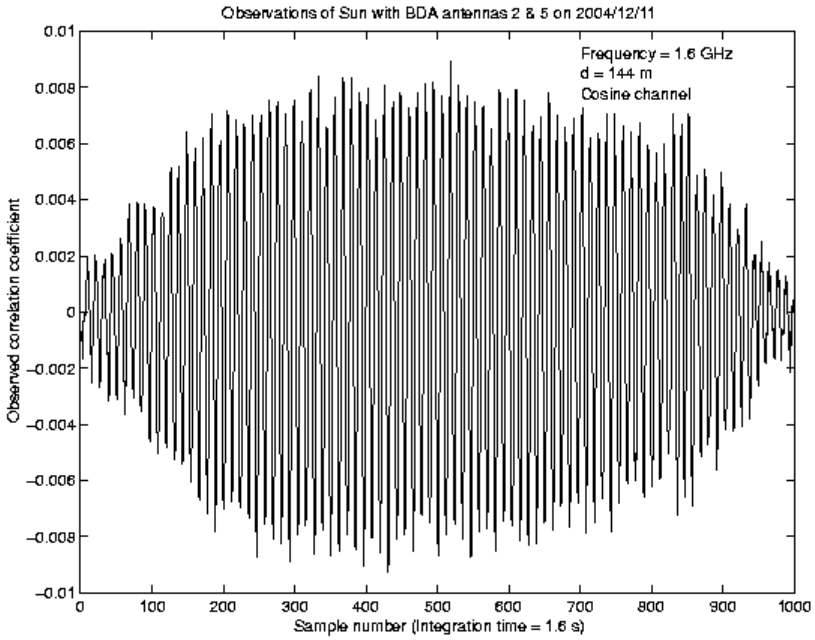

FIGURE 6.34 – Cosine fringe obtained on 11/12/2004 throughout the interferometer pair composed of A2 and A5 antennas in the observation of Sun.

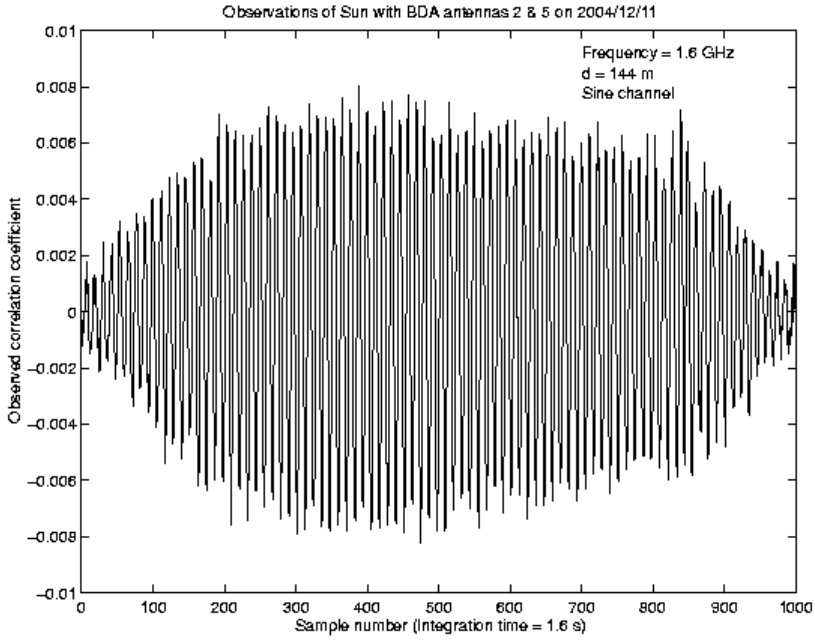

FIGURE 6.35 – Sine fringe obtained on 11/12/2004 throughout the interferometer pair composed of A2 and A5 antennas in the observation of Sun.

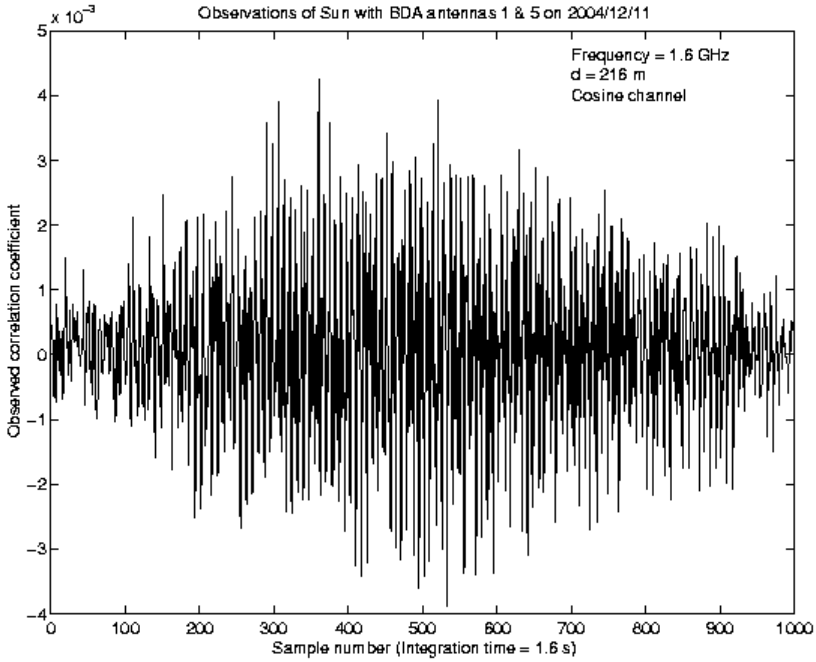

FIGURE 6.36 – Cosine fringe obtained on 11/12/2004 throughout the interferometer pair composed of A1 and A5 antennas in the observation of Sun.

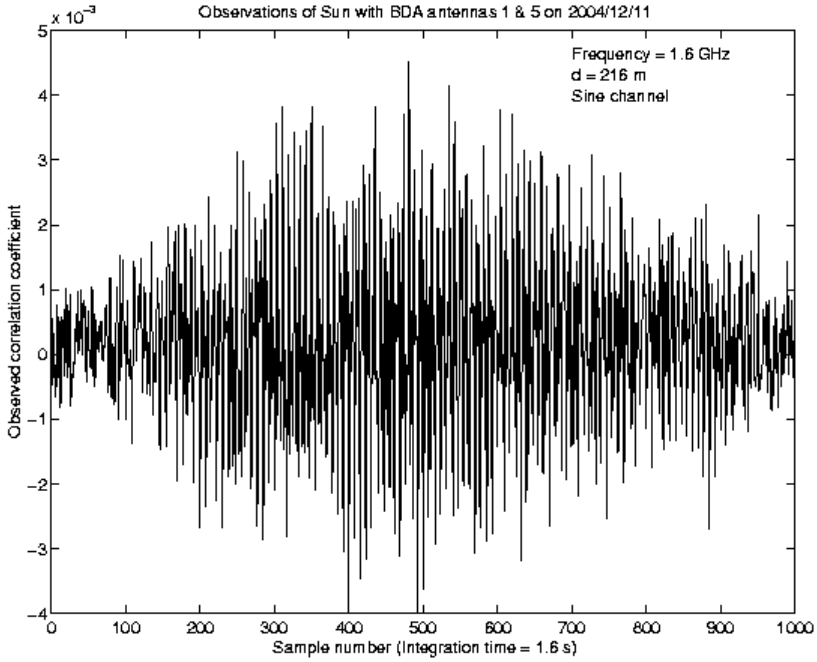

FIGURE 6.37 – Sine fringe obtained on 11/12/2004 throughout the interferometer pair composed of A1 and A5 antennas in the observation of Sun.

REFERENCES

Aschwanden, M. J.; Benz, A. O.; Dennis, B. R.; Schwartz, R. A. Solar Electron Beams Detected in Hard X-Rays and Radio Waves **Astrophysical Journal,** v. 455, p. 347, 1995.

Bastian, T. S.; Gopalswamy, N.; Shibasaki, K. Solar Physics with Radio Observations. **NRO Report**, v. 479, 1999. Proceedings of the Nobeyama Symposium (1998).

Beauchamp, K. G. Walsh function and thier applications**.** London: Academic Press, 1975.

Botti, L. C. L.; Abraham, Z. Longterm Radio Observations of the Nucleus of NGC5128 Centaurus-A. **Monthly Notices of the Royal Astronomical Society**, v. 264, n. 4, p. 807-812, 1993.

Brueckner, G. E.; Howard, R. A.; Koomen, M. J.; Korendyke, C. M.; Michels, D. J.; Moses, J. D.; Socker, D. G.; Dere, K. P.; Lamy, P. L.; Llebaria, A.; Bout, M. V.; Schwenn, R.; Simnett, G. M.; Bedford, D. K.; Eyles, C. J. The Large Angle Spectroscopic Coronagraph (LASCO). **Solar Physics**, v. 162, n. 2, p. 357-402, 1995.

Cecatto, J. R., **Radiômetro milimétrico de alta resolução e fragmentação temporal de fulgurações solares durante a fase impulsiva**. 185 p. (INPE-6126-TDI/587) Tese (Doutorado em Astrofísica) – Instituto Nacional de Pesquisas Espaciais, São José dos Campos. 1996.

Cecatto, J. R.; Sawant, H. S.; Fernandes, F. C. R.; Krishan, V.; Neri, J. A. C. F.; Moraes Filho, J. C. High resolution time profile of decimetric type-III bursts. **Advances in Space Research**, v. 32, n. 12, p. 2533-2537, 2003.

Cecatto, J R; Fernandes, F. C. R.; Neri, J A C F; Bethi, N; Felipini, N S; Madsen, F R H; Andrade, M C; Soares, A C; Alonso, E M B; Sawant, H S. Protótipo do primeiro interferômetro brasileiro (Projeto Brazilian Decimetric Array – BDA). **Boletim da Sociedade Astronômica Brasileira**, v. 23, n. 3, p. 25-38, 2004.

Clark, B. G. An efficient implementation of the algorithm `CLEAN´. **Astronomy and Astrophysics,** v. 89, n. 3, p. 377-378, 1980.

Cornwell, T. J. A novel principle for optimization of the instantaneous fourier plane coverage of correlation arrays. **IEEE Transations Antenna Propagation.** v. 36, p. 1165–1167, 1988.

Faria, C.; Sawant, H. S.; Stephany, S. Solar Radio Observations with High Spatial Resolution. In: Workshop dos Cursos de Computação Aplicada do INPE, IV. (WORCAP), 20-21 October, 2004, São José dos Campos. **Anais...** São José dos Campos: LAC/INPE. CD-ROM.

Fernandes, F. C. R., **Espectrógrafo decimétrico de alta sensibilidade e resolução: análise preliminar das explosões solares**. 132 p. (INPE-5537-TDI/525) Dissertação (Mestrado em Ciência Espacial - Radioastronomia e Física Solar) - Instituto Nacional de Pesquisas Espaciais, São José dos Campos. 1992.

Fernandes, F. C. R., **Espectrógrafo Digital Decimétrico de banda larga e investigações de flares solares em rádio e raios-X**. 178 p. (INPE-6396-TDI/612) Tese (Doutorado em Astrofísica) - Instituto Nacional de Pesquisas Espaciais, São José dos Campos. 1997.

Fernandes, F. C. R.; Cecatto, J. R.; Neri, J. A. C. F.; Faria, C; Martinon, A. R. F.; Rosa, R. R.;

Mesquita, F. P. V.; Portezani, A.; Andrade, M. C.; Alonso, E. M. B.; Vats, H. O.; Sawant, H. S. O Brazilian Solar Spectroscope (BSS) e os Problamas Atuais da Física Solar. **Boletim da Sociedade Astronômica Brasileira**, v. 20, n. 2, p. 33-43, 2000a.

Fernandes, F. C. R.; Sawant, H. S.; Melendez, J. L.; Benz, A. O.; Knane, S. R. Investigations of the Acceleration Region of Energetic Electrons Associated with Decimetric Type III and X-Ray Bursts. **Advances in Space Research**, v. 25, n. 9, p. 1813-1816, 2000b.

Fleck, B.; Domingo, V.; Poland, A. The SOHO mission, Dordrecht: Kluwer, 1995, edited by Fleck, B.; Domingo, V.; Poland, A.

Hogbom, J. Aperture synthesis with a non regular distribution of interferometer baselines. **Astronomy and Astrophysics Supplement**, v. 15, n. 1, p. 417-426, 1974.

Janardhan, P., Fujiki, K., Kojima, M., Tokumaru, M., and Hakamada, K. Resolving the Enigmatic Solar Wind Disappearance Event of 11 May 1999. **Jou. Geophys. Res**.110, A08101, 2005.

Janardhan, P. , Enigmatic solar wind disappearance events: Do we understand them?. **Jou. Astrophys. Astron.** 27, 1-7, 2006.

Jaynes, E. T. Information Theory and statistical mechanics. **Physical Review,** v. 106, n. 1, p. 620-630, 1957.

Jennison, R. C. A phase sensitive interferometer technique for the measurement of the Fourier transforms of spatial brightness distributions of small angular extent. **Monthly Notices of the Royal Astronomical Society,** v. 118, n. 1, p. 276, 1958.

Keto, E., The shapes of cross-correlation interferometers. **Astrophysical Journal,** v. 475, p. 843-852, 1997.

Kogan, L. Optimizing a large array configuration to minimize the sidelobe. **IEEE Trans. Antenna Propagation,** v. 48, p. 1075-1078, 2000.

Kuehr, H.; Witzel, A.; Pauliny-Toth, I .I. K.; Nauber, U. A catalogue of extragalactic radio sources having flux densities greater than 1 Jy at 5 GHz. **Astronomy and Astrophysics Supplement Series**, v. 45, p. 367-430, 1981.

Nakajima, H.; Nishio, M.; Enome, S.; Shibasaki, K.; Takano, T.; Hanaoka, Y.; Torii, C.; Sekiguchi, H.; Bushimata, T.; Kawashima, S.; Shinohara, N.; Irimajiri, Y.; Koshiishi, H.; Kosugi, T.; Shiomi, Y.; Sawa, M; Kai, K. The Nobeyama radioheliograph, **Proc. IEEE,** v. 82, n. 5, p. 705-713, 1994.

Nakajima, H.; Nishio, M.; Enome, S.; Shibasaki, K.; Takano, T.; Hanaoka, Y.; Torii, C.; Sekiguchi, H.; Bushimata, T.; Kawashima, S.; Shinohara, N.; Irimajiri, Y.; Koshiishi, H.; Kosugi, T.; Shiomi, Y.; Sawa, M.; Kai, K. New Nobeyama Radio Heliograph. **Astrophysics & Astronomy Supplement,** v. 16, n. 1, p. 437, 1995.

Narayan, R.; Nityananda, R. Maximum entropy image restoration in astronomy. **Annual Review of Astronomy and Astrophysics,** v. 24, n. 1, p. 127-170, 1986.

Pearson, T. J.; Readhead, A. C. S. Image Formation by Self-Calibration in Radio Astronomy. **Annual Review of Astronomy and Astrophysics**, v. 22, n, 1, p. 97-130, 1984.

Press, W .H. **Numerical Recipes in Fortran** – Second Edition, University Press, 1992, p. 51.

Ramaty, R.; Mandzhavidze N. High Energy Solar Physics Workshop - Anticipating HESSI, **Astronomical Society of the Pacific Conference Series,** v. 206, n. 1, 2000. Special issue on the Anticipating HESSI Workshop - 2000.

Ramesh, R., Bangalore, Índia. Ph.D. Thesis - Bangalore University, 1998.

Ramesh, R.; Subramanian, K. R.; Sundara Rajan; M. S.; Sastry, Ch. V. The Gauribidanur Radioheliograph. **Solar Physics,** v. 181, n. 2, p. 439-453, 1998.

Ramesh, R.; Subramanian, K. R.; Sastry, Ch. V. Phase calibration scheme for a "T" array. **Astronomy and Astrophysics Supplement Series,** v. 139, n. 1, p. 179-181, 1999.

Ramesh, R., Sawant, H. S., Cecatto, J. R., Faria, C., Fernandes, F. C. R., Madsen, F. R. H., Kathiravan, C., Suryanarayana, G. S. Brazilian Decimetre Array (Phase–1): Initial Solar Observations. **Advances in Space Research,** 2007 (Accepted).

Readhead, A. C. S.; Wilkinson, P. N. The mapping of compact radio sources from VLBI data. **Astrophysical Journal,** v. 223, n. 1, p. 25-36, 1978.

Rogstad, D. H. A technique for measuring visibility phase with an optical interferometer in the presence of atmospheric seeing. **Applied Optics IP**, v. 7, n. 4, p. 585, 1968.

Rosa, R. R.; Sawant, H. S.; Valdivia, J. A.; Sharma, A. S. Dissipative Structure And Weak Turbulence In The Solar Corona. **Advances in Space Research,** v. 20, n. 12, p. 2303-2308, 1997.

Rosa, R. R.; Sawant, H. S.; Cecatto, J. R.; Rodrigues Neto, C.; Lopes, V. C. A.; Subramanian, K. R.; Fernandes, F. C. R.; Saito, J. H.; Moron, C. E.; Mucheroni, M. L.; Furuya, N.; Mascarenhas, N. Phenomenological Dynamics of Coronal Loops by using a Neural Network Approach. **Advances in Space Research**, v. 25, n. 9, p. 1917-1921, 2000a.

Rosa, R. R.; Sawant, H. S.; Costa Junior, R. A.; Ramos, F. M.; Cecatto, J. R.; Fernandes, F. C. R.; Saito, J. H.; Moron, C. E.; Mucheroni, M. L. Normalized Emission Measurement - Density Curves of X-ray Loop. **Astronomical Society of the Pacific Conference Series**, v. 206, n. 1, p. 293-296, 2000b.

Rosa, R. R.; Vats, H. O.; Ramos, F. M.; Zanandrea, A.; Rodrigues Neto, C.; Fernandes, F. C. R.; Bolzan, M. J. A.; Rempel, E. L.; Brito, R. C.; Vijaykumar, N. L.; Sawant, H. S. Characterization of local self-similarity and criticality in the solar active regions **Advances in Space Research**, v. 29, n. 3, p. 463-468, 2002.

Saito, J. H.; Rosa, R. R.; Sawant, H. S. Máquina Paralela de DSPs para tomografia espectral solar. In: Workshop para Assessoria da FINEP (WA FINEP), 1996, São Paulo. **Livro de Resumo...** p.20, 1996.

Sawant, H. S.; Lattari, C. J. B.; Benz, A. O.; Dennis, B. R. Hard X-rays and associated weak decimetric bursts. **Solar Physics,** v. 130, p. 57-73, 1990.

Sawant, H. S.; Rosa, R. R. High sensitivity, high frequency and high time resolution decimetric spectroscope. **Revista Mexicana de Astronomia y Astrofísica,** v. 21, n. 1, p. 651-654, 1990.

Sawant, H. S.; Sobral, J. H. A.; Neri, J. A. C. F.; Fernandes, F. C. R.; Rosa, R. R.; Cecatto, J. R.; Martinazzo, D. High sensistivity, high frequency and high time resolution decimeter solar

radio spectroscope In: Reunião Anual da SBPC, 43., 1991, Rio de Janeiro, RJ. **Anais...**. Rio de Janeiro: Ed. SBPC, 1991. p. 689-690. ISSN 0102-2474.

Sawant, H. S.; Rosa, R. R.; Cecatto, J. R.; Fernandes, F. C. R. High Spectral Resolution of mm-Wavelength (23-18) GHz Solar Burst. **Lecture Notes in Physics,** v. 399, n. 1, p. 367, 1992a.

Sawant, H. S.; Sobral, J. H. A.; Neri, J. A. C. F.; Fernandes, F. C. R.; Rosa, R. R.; Cecatto, J. R.; Martinazzo, D. Decimeter High Resolution Solar Radio Spectroscope. **Lecture Notes in Physics**, v. 399, n. 1, p. 318-321, 1992b.

Sawant, H. S.; Sobral, J. H. A.; Neri, J. A. C. F.; Fernandes, F. C. R.; Cecatto, J. R.; Rosa, R. R. High Sensitivity Digital Decimetric Spectroscope. **Advances in Space Research**, v. 13, n. 9, p. 199-202, 1993.

Sawant, H. S.; Cecatto, J. R. High-Sensitivity Spectral Resolution mm-Wavelength (18-23 GHz) Radiometer. **Solar Physics**, v. 150, n. 2, p. 375-384, 1994.

Sawant, H. S.; Sobral, J. H. A.; Fernandes, F. C. R.; Cecatto, J. R.; Day, W. R. G.; Neri, J. A. C. F.; Alonso, E. M. B.; Moraes, A. High Sensitivity Wide Band Digital Solar Polarimetric Spectroscope. **Advances in Space Research**, v. 17, n. 4/5, p. 385-388, 1996.Sawant, H. S.; Subramanian, K. R.; Faria, C.; Stephany, S.; Fernandes, F. C. R.; Cecatto, J. R.; Rosa, R. R.; Portezani, V. A.; Mesquita, F. P. V.; Alonso, E. M. B. Data Acquisition and Recent Results of the Brazilian Solar Spectroscope - BSS. **Astronomical Society of the Pacific Conference Series**, v. 206, n. 1, p. 347-350, 2000a.

Sawant, H. S.; Ludke, E.; Subramanian, K. R.; Cecatto, J. R.; Fernandes, F. C. R.; Rosa, R. R.; Sobral, J. H. A.; Swarup, G.; Scalise, E.; Boas, J. W. V. A High Resolution Decimetric Solar. Radioheliograph. **Astronomical Society of the Pacific Conference Series**, v. 206, n. 1, p. 341-346, 2000b.

Sawant, H. S.; Subramanian, K. R.; Lüdke, E.; Sobral, J. H. A.; Swarup, G.; Fernandes, F. C. R.; Rosa, R. R.; Cecatto, J. R. Brazilian Decimetric Array. **Advances in Space Research,** v. 25, n. 9, p. 1809-1812, 2000c.

Sawant, H. S.; Subramanian, K. R.; Faria, C.; Fernandes, F. C. R.; Sobral, J. H. A.; Cecatto, J. R.; Rosa, R. R.; Vats, H. O.; Neri, J. A. C. F.; Alonso, E. M. B.; Mesquita, F. P. V.; Portezani, A.; Martinon, A. R. F. Brazilian Solar Spectroscope (BSS). **Solar Physics**, v. 200, n. 1-2, p. 167-176, 2001.

Sawant, H. S.; Neri, J. A. C. F.; Fernandes, F. C. R.; Cecatto, J. R.; Sankararaman, M. R.; Faria, C.; Subramanian, K. R.; Sundararajan, M. I. S.; Ramesh, R.; Karlický, M.; Southern Hemisphere Solar Radio Heliograph. **ESA SP,** v. 506, n. 2, p. 971-974, 2002. Special issue on the 10th European Solar Physics Meeting.

Sawant, H. S.; Neri, J. A. C. F.; Fernandes, F. C. R.; Cecatto, J. R.; Sankararaman, M. R.; Faria, C.; Stephany, S.; Rosa, R. R.; Andrade, M. C.; Alonso, E. M. B.; Lüdke, E.; Subramanian, K. R.; Ramesh, R.; Sundararajan, M. S.; Ananthakrishnan, S.; Swarup, G.; Boas, J. W. V.; Botti, L. C. L.; Moron, C. E.; Saito, J. H. A low cost steerable radio-telescope, **Advances in Space Research**, v. 32, n. 12, p. 2715-2720, 2003.

Sawant, H. S., C. Faria, J. R. Cecatto, F. C. R. Fernandes**,** L. F. S. Cicconello, A. B. Cassiano, S. Stephany, R. R. Rosa, F. R. H. Madsen, K. R. Subramanian, R. Ramesh, M. S. I. Sundararajan, Brazilian Decimetric Array, **Proc. URSI-GA,** 2005 (www.ursi.org/Proceedings/ProcGA05/pdf/J05-P.12(01578).pdf).

Sawant, H.S. R. Ramesh, J.R. Cecatto, C. Faria, F.C.R. Fernandes, R.R. Rosa, M.C. Andrade, F.R.H. Madsen, S. Stephany, L.B.T. Cividanes, C.A.I. Miranda, L.C.L. Botti, J. W.S.V. Boas, J.H. Saito, C.E. Moron, N.D. Mascarenhas, K.R. Subramanian, M.S. SundaraRajan, E. Ebenezer, M.R. Sankararaman. Prototype of the Brazilian Decimetric Array. **Solar Physics** 2007 (Accepted).

Swarup, G. Personal comunication, 1990.

Swarup, G. Personal comunication, 1991.

Thompson, A. R., Moran, J. M., Swenson Jr., G. W. **Interferometry and Synthesis in Radio Astronomy.** New York: Wiley, 1994.

Udaya Shankar, N. **Application of digital techniques to radio astronomy measurements.** Bangalore, Índia. Ph. D Thesis – Raman Research Institute, University of Banglore, 1986.

Van Vleck, J. H.; Middleton, D. **Proc. IEEE**, v. 54, n. 1, p. 2, 1966.

Weinreb, S. **A digital spectral analysis thechnique and its application to radio astronomy**. Ph.D. Thesis - Dept. Electrical Engineering, Massachusetts Institute of Technology - MIT, Cambridge, MA, USA. 1963.

Wohlenben, R.; Mattes, H.; Krichbaum, J. **Interferometry in radioastronomy and radar techniques.** Dordrecht, Netherlands: Kluwer, 1991, 210 p.

Zirin, H.; Baumert, B. M.; Hurford, G. J. The microwave brightness temperature spectrum of the quiet sun. **Astrophysical Journal,** v. 370, n. 1, p. 779-783, 1991.